Master Thesis

submitted within the UNIGIS MSc. programme
at the Department of Geoinformatics - Z_GIS
University of Salzburg, Austria
under the provisions of the UNIGIS framework

Geospatial analysis of Landslide Susceptibility in Panauti Municipality, Central Nepal Lesser Himalaya

By

Arju Bhattarai
U106959

A thesis submitted in partial fulfilment of the requirements of
the degree of
Master of Science (Geographical Information Science & Systems) – MSc (GISc)

Advisor (s):

Dr HimLal Shrestha

Kathmandu, March 12, 2024.

Science Pledge

By my signature below, I certify that my thesis report is entirely the result of my own work. I have cited all sources of information and data I have used in my project report and indicated their origin.

Kathmandu, Nepal/ March,2024

Place and Date	Signature

Acknowledgment

First and foremost, I am grateful to the University of Salzburg for offering the "Master of Science (Geographic Information System)" course in Nepal. The MSc (GIS) department and KAFCOL college staff have made significant contributions to the successful operation of the program at KAFCOL.

I am grateful to my supervisor, Dr. Him Lal Shrestha, for patiently guiding me through my MSc journey. Working under his supervision was a privilege, and I am grateful for his advice, encouragement, constructive input, and editorial ideas. He prioritized my work and provided ongoing encouragement and training. His commitment to my academic growth extended beyond the classroom, as he ventured into the field with me, sharing his expertise and experience. His regular updates and encouragement prepared me for the final defense, and I am truly grateful for his unmatched dedication.

I also want to express my profound gratitude to Panauti Municipality for supporting me financially and motivating me to do my thesis work in the Panauti Municipality Area.

Special Thanks to my colleagues Ms. Shristi Shakya, Mr. Asim Timalsina, Ms. Deepa Dahal, and Mr. Ananta Poudel for supporting and encouraging me and our UNIGIS Faculty Members Dr. Upama Koju, Dr. Ambika Prasad Gautam, and Mr. Prasid Kandel for making my learning journey in KAFCOL fruitful.

I am grateful to my family, my father and mother, who have always encouraged me to seek my university degree and provided a conducive study atmosphere both inside and outside the home.

Abbreviations

AHP	Analytical Hierarchical Process
FR	Frequency Ratio
LULC	Land Use Land Cover
DIPS	Software for kinematics analysis
CI/CR	Consistency Index/Ratio
AUC	Area Under Curve
DEM	Digital Elevation Model
LSM	Landslide Susceptibility Maps
ROC	Receiver Operating Characteristics
TWI	Topographic Wetness Index
WGS	World Geodetic System
UTM	Universal Transverse Mercator
mm	Millimeter
Km	Kilometer
DMG	Department of Mines and Geology
RF	Relative Frequency
LSI	Landslide Susceptibility Index
PR	Prediction Rate

Abstract:

Landslide susceptibility mapping (LSM) plays a crucial role in both development planning and disaster management. Using Geographic Information Systems (GIS) and remote sensing techniques, LSM integrates various causative factors to predict areas prone to slope instability. This research is done to process LSM maps using both the Hierarchical and Quantitative approach i.e. Analytical Hierarchical Process (AHP) Method and the Frequency Ratio (FR) Method. The study area consists of 1, 2, 3, 8, and 12 wards of Panauti Municipality. Ten causative factors including slope, slope aspect, curvature, land use/land cover (LULC), lithology, distance from river and drainage, distance from fault lines, topographic wetness index (TWI), and precipitation were integrated into the LSM framework. High-resolution satellite imagery coupled with field verification identified 138 landslides, partitioned into training (70%) and validation (30%) datasets. This comprehensive approach, combining GIS, remote sensing, and statistical techniques, not only facilitates accurate LSM but also offers insights into potential landslide scenarios and the efficacy of mitigation measures. Our findings underscore the importance of integrating diverse datasets and methodologies for robust Landslide Susceptibility Mapping.

The resulting LSM map was categorized into five susceptibility indices: Very High, High, Moderate, Low, and Very Low. This classification enabled the identification of areas highly susceptible to landslides, crucial for implementing effective mitigation strategies. Moreover, kinematic analyses of major landslides facilitated the calculation of failure probabilities, enhancing our understanding of slope instability dynamics. By comparing the performance of these methods using metrics such as the density of landslide pixels and ROC/AUC curve analysis, the study evaluates the effectiveness of each approach. The findings indicate that the Frequency Ratio method outperforms the Analytical Hierarchy Process method, achieving higher accuracy in predicting landslide susceptibility. The success rate of FR is 85.2 % whereas AHP is 75.4%.

Table of Contents

Science Pledge ii
Acknowledgment iii
Abbreviations iv
Abstract: v
CHAPTER 1: Introduction 12
1.1 Background: 12
1.2 Location and Accessibility: 13
1.3 Climate and Vegetation 15
1.4 Topography and Drainage 15
1.5 Problem Statement of the Study Area 16
1.6 Research Questions 17
1.7 Objectives 17
1.7.1Main Objectives 17
Specific Objectives 18
1.8 Limitations 18
CHAPTER 2: Literature Review 19
2.1 Review in Landslide and Landslide Susceptibility mapping 19
2.2 Review related Geology of Central Lesser Himalaya Nepal 21
2.3 Review on LSM using various methods 23
CHAPTER 3: Materials and Methodology 26
3.1 Data Used 26
3.1.1 Grid Size and Coordinate System Projection Used: 28
3.1.3 Image Processing 28
3.1.4 Data Processing 28
3.2 Software used: 29
3.3 Desk study 29
3.4 Field study 30
3.5 Landslide Inventory mapping: 30
3.6 Slope Stability Analysis Using DIPS: 30
3.7 Data analysis: 31
3.7.1 Slope: 31
3.7.2 Slope Aspect 31
3.7.3 Lithology: 32
3.7.4 Distance from Road 32

3.7.5 Distance from Fault 32
3.7.6 Distance from Drainage 33
3.7.7 Land Used Land Cover 33
3.7.7.1 Accuracy Assessment of Land Use Land Cover 33
3.7.8 Precipitation 34
3.7.9 Curvature 34
3.7.10 Topographic Wetness Index (TWI) 34
3.8 Landslide Susceptibility Mapping 35
3.8.1 Analytical hierarchy method: 35
3.8.2 Landslide Susceptibility Index from AHP Method: 37
3.8.3 Frequency Ratio Model: 37
3.8.4 Landslide Susceptibility Index from Frequency Method 38
8.5 Validation: 38
3.9 Methodological Frame Work of the Study area 40
CHAPTER 4: Results 41
4.1 Litho stratigraphy of the study area: 41
4.1.1 Faults: 41
4.1.2 S fold: 41
4.1.3 Fold: 42
4.2 Landslide Investigation 43
4.2.1 Debris flow 43
4.2.2 Rock fall 44
4.2.3 Kinematics analysis 45
4.3 Landside inventory Map 46
4.4 Factors Affecting Landslide 48
4.4.1. Slope 48
4.4.2 Slope Aspect: 50
4.4.3 Lithology 51
4.4.4 Road: 53
4.4.5 Fault: 54
4.4.6 Drainage: 55
4.4.7 Land Use Land Cover 56
4.4.8 Rainfall: 57
4.4.9 Topographic Wetness Index (TWI) 58
4.4.10 Slope curvature: 59
4.4 Landslide Susceptibility Mapping 61

4.5.1 Analytical Hierarchy Process Method 61
4.5.2 Landslide Susceptibility Map from AHP Method: 67
4.5.3 Frequecy Ratio Method: 69
4.5.4 Landslide Susceptibility Map from Frequency Ratio Method: 58
4.5.5 Comparison Based on Landslide Density 59
4.5.5 Validation of FR and AHP method 59
CHAPTER 5: Discussions 61
5.1 Pros and Cons of FR and AHP method 63
5.2 Recommendation 63
CHAPTER 6: Conclusions 66
References: 67

List of Figures

Figure 1: Location Map of the Study Area. 14
Figure 2: Drainage Map of the Study Area. 16
Figure 3: Division of Nepal Himalaya into 5 tectonic zone by Gansser, 1964 and Hagen, 1969....22
Figure 4: Methodological Frame Work of the Study Area 40
Figure 5: The map representing the point location of the data collection for kinematic analysis....45
Figure 6: Map indicating testiong and training dataset of the study area....47
Figure 7: Map after digitizing landslide area in Polygon....48
Figure 8: The Map representing slope of the study area....49
Figure 9: Slope Aspect Map of the study area....50
Figure 10: The map representing Lithology of Study area. 52
Figure 11: The map representing Euclidean Distance of Road with the study area Boundary. 53
Figure 12: The Map representing Euclidean Distance of Fault within the Boundary of Study area....54
Figure 13: The Map representing Euclidean Distance of Drainage within the Boundary of Study area....55
Figure 14: The map representing the Land Use Land Cover Map of the study area. 56
Figure 15: Average Annual precipitation map of the study area (2010-2012) 58
Figure 16: Map representing Topographic Wetness Index of study area 59
Figure 17: Map showing the curvature of the study area. 60
Figure 18: Bar graph representing the factors in corresponding to their weightage 62
Figure 19: Landslide Susceptible map From AHP Method 67
Figure 20: Landslide Susceptible Map from Frequency Ratio Method 58
Figure 21: AUC Curve for validation of Map from AHP method 60
Figure 22: AUC Curve for validation of Map from Frequency Ratio method....60

List of Tables

Table 1: Background Details of Panauti Municipality 14
Table 2: Datasets used, its Description, Source and Type.....27
Table 3: The software used with its purpose. 29
Table 4: Division of landslide point datasets. 30
Table 5: Matrix of pairwise comparison (Saaty, 2000) 36
Table 6: The basic scale of preference between two variables for pairwise comparison matrix in AHP method (Saaty et al., 2001). 36
Table 7: The categorization of ROC Curve Value. 39
Table 8: Details of possible failure in Landslide prone area. 46
Table 9: Landslides in each classes of Slope 49
Table 10: Landslide distribution with respect to each aspect classes 51
Table 11. Landslide distribution with respect to each Formation. 52
Table 12: Landslide distribution in each classes of Euclidean Road distance 53
Table 13: Landslide distribution in each classes of Euclidean Fault distance 54
Table 14: Landslide distribution in each classes of Euclidean Drainage Distance 55
Table 15: Landslide distribution in each classes of Land Use Land Cover.....56
Table 16: Accuracy Assessment of Land Use Land Cover Map 57
Table 17: Landslide in 5 different classes of Precipitation. 58
Table 18: Landslide in different classes of Topographic Wetness Index 59
Table 19: Landslide Present in each classes of slope curvature.....60
Table 20: The pair-wise comparison matrix, class weights (rating) and consistency ratio....61
Table 21: The pair-wise comparison matrix, class weights (rating) and consistency ratio....63
Table 22: The distribution of landslide susceptibility zones and landslide occurrence.....68
Table 23 : Frequency ratio of 10 causative factors 69
Table 24: The distribution of landslide susceptibility zones and landslide occurrence.....58
Table 25: The landslide densities of the susceptibility classes of both the LSM maps 59

List of Photographs

Photograph 1: S-type fold observed in field work near Roshi Khola area 31
Photograph 2: Fold observed during field work up to the Nagidada hill. 31
Photograph 3: Debris flow at nagi dada showing failure of mitigation measure 32
Photograph 4: Landsldie due to road cutting in the study area. 33
Photograph 5: Rock fall chances in the mining sites near Roshi Khola. 33

CHAPTER 1: Introduction

1.1 Background:

The Indian and Eurasian plates collided to create the Himalayas, one of the planet's youngest mountain ranges. One-third of the Himalayan arc is made up of Nepal, which is located in the center region of the Himalayan range. The complicated geology a range of climate conditions and floral richness within a constrained range of elevations distinguish Nepal as a special location on Earth. But because of its unique physiography and biogeography which are the result of hydrologic, tectonic, seismic, and geomorphologic processes it is now more susceptible to natural disasters (Hasegawa et al., 2009).

The intricate interactions between natural and artificial causes, the midland areas have been particularly vulnerable to landslides. Due to a unique combination of factors including high rates of weathering and abundant rainfall, together with an active tectonic setting, growing urbanization, and infrastructure development, landslides constitute a major natural hazard in Nepal. Furthermore, the problem of landslides has gotten worse in Nepal and worldwide as a result of both an increase in the frequency of extreme events and climate change. Natural disasters include landslides, which are catastrophic events that result in significant losses of life, property, and other infrastructure and are beyond human control. However, the effects of landslides also overlap with those of conflict or war. A variety of trigger mechanisms and susceptibility factors, including rainfall, earthquakes, vegetation degradation, steep slopes, harsh terrain, changing climatic and microclimatic conditions, and fragile and complex geology, combine to cause landslides (Gerrard et al., 2002). In Nepal, the susceptibility to landslides varies by area. Rainfall and this fluctuation are frequently closely correlated. Almost every year during the monsoon, landslides caused by rainfall occur, and the amount of rainfall varies across Nepal (Kansakar et al., 2004).

In general, geological, hydrological, and atmospheric phenomena such as landslides, floods, earthquakes, and volcanoes are the causes of socioeconomic disturbance. The movement of a mass of rock, debris, or earth down a slope is referred to as a landslide (Cruden, 1991). Landslides can be caused by several external stimuli, including strong rains, shaking from an earthquake, changes in water level, storm waves, or rapid stream erosion that causes a rapid increase in shear stress or decrease in the shear strength of materials that form slopes. The main causes of surface soil's increased sensitivity to instability include overuse of natural

resources, deforestation, and expanding urbanization, and unregulated land use, which also increases the vulnerability of the exposed population. Existing landslides can be categorized as active, dormant (perhaps revived), or inactive (typically relict or fossil) based on their level of activity or movement. It might happen one at a time or in clusters of up to thousands. For instance, several landslides happen practically at the same time, when an earthquake shakes the slopes, or over several hours or days when heavy rains or snowmelt cause failures (Guzzetti et al., 2005).

By identifying slopes with a high failure risk, landslide susceptibility mapping facilitates the making of the necessary protective and preventive actions (Guillard and Zezere, 2012). It is accurate to define landslide susceptibility zonation as the dividing the earth's surface into zones that are almost uniform in size and classifying them based on the level of landslide risk that is present or predicted. The premise behind all currently available techniques for mapping landslide susceptibility is that similar conditions to those that caused and continue to cause landslides in the past and present, in terms of geology, geomorphology, hydrogeology, and climate, increase the likelihood of landslides occurring in the future. Both field surveys and the analysis of remote sensing images can be used to classify, identify, categorize, and map the geomorphological features of landslides. These features are controlled by observable internal factors (i.e. inherent characteristics of the ground), known as causative factors, which can also be mapped from field surveys and remote sensing image interpretations.

1.2 Location and Accessibility:

Panauti is a relatively small municipality in Kavrepalanchowk district of Bagmati zone of central development region. The municipality lies 32 kilometers east from Kathmandu and immediately south of Banepa Municipality (Panauti Municipality, 2024). The main source of income here is agriculture. The study area is comprised of 5 wards within the Panauti municipality, spatial extent between 27°32’ to 27°38’ north latitude and 85°24’ to 85°30’ east longitude. Potato, paddy, orange, milk are the main agricultural products. Besides these people have taken small scale industries, business, and animal husbandry as the source of income (Panauti Municipality, 2024). Panauti is bordered by Sharada Batase, Shankhupati Chaur VDC and Dhulikhel Municipality on the east; Kushadevi, Mahendrajyoti VDC on the west; and Banepa Municipality on the north; and Kalati Danda, Chalal Ganesthan and Balthali VDC on the south (Panauti Municipality, 2024).

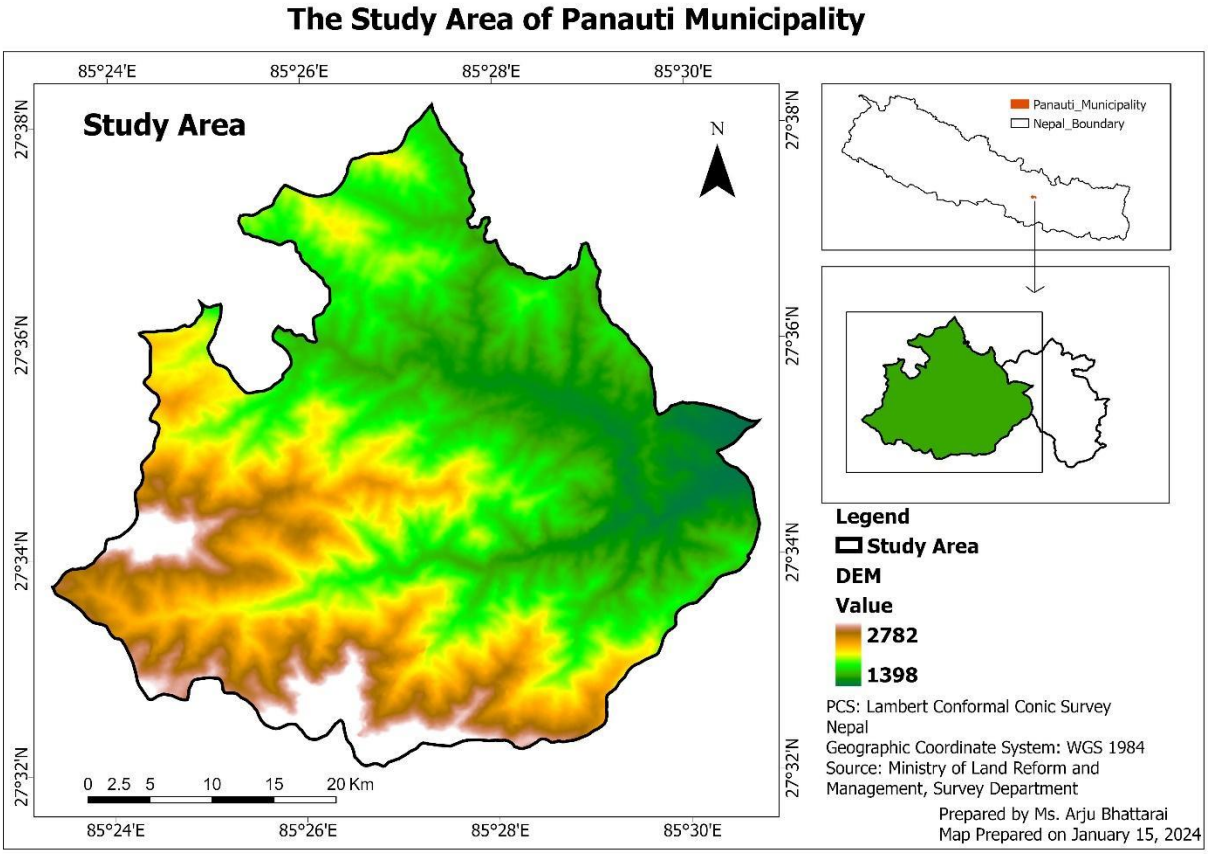

Figure 1: Location Map of the Study Area.

General details about Panauti Municipality is given in Table 1.

Table 1: Background Details of Panauti Municipality

Descriptions	**Details**
District	Kavrepalanchwok
Number of wards	12
Population (2011)	56329
Area	118.09 sq. km.
Average Rainfall	1200 mm
Min-Max temperature	0-32 degree Celsius

Major geological structure such as faults, folds, and thrusts that characterize the Himalayan mountain range provide evidence of its creation. In Kushadevi (Nagi Dada), the majority of the rocks are sedimentary and metamorphic nature. The local tectonic activity has caused

these rocks to fracture and fold. The region's tectonic activity has resulted in folding and faulting. Sedimentary rocks, such as sandstones, siltstones, and shales, were deposited during the Jurassic and Cretaceous periods. Metamorphic rocks, such as gneisses, granites, and schists, are products of the intense heat and pressure that go into the development of mountains. Due to the steep terrain and deterioration of the rocks, the region is also vulnerable to landslides and rock falls. A landslide that happened in the neighboring Sindhupalchowk area in 2014 resulted in significant damage and fatalities. In conclusion, the tectonic activity linked to the Himalayan mountain range has shaped the geology of Kushadevi. Complex geological structures and a combination of sedimentary and metamorphic rocks are features of the region. The steep terrain and weathering of the rocks make the area prone to landslides and rock falls, which can have significant impacts on the local communities (Bhandari et al., 2015).

1.3 Climate and Vegetation

Climatic conditions are mainly influenced by the geographical aspects such as elevation and topography. The fluctuations in both the temperature and precipitation are due to a wide variation in elevation. Commonly the monsoon starts from June and end in the last week of the September that contribute more than 70-80 percentage of the total annual rainfall of the area.

In general, it is known for its diverse vegetation due to its varying topography, ranging from lowland Terai to the high Himalayas. Common vegetation types in Nepal include subtropical forests, temperate forests, and alpine vegetation. The average annual rainfall of the given area is 1200 mm (Panauti Municipality, 2024).

1.4 Topography and Drainage

The stream, called Roshi Khola, is fed by springs and has several tributaries, including Muldole, Sishakhani, Baira Mahadev, Gudgude, and Khar Khola. It flows from west to southeast and eventually joins the Lilawati Khola at Bhaleshwor Dobhan and Punyamata Khola at Pathani Triveni Ghat, which is a tributary of the Sunkoshi River in south central Nepal. Roshi Khola (Panauti), situated 5 km southeast of the catchment region and at an elevation of 1480 meters above mean sea level (27˚34’50” N and 85˚30’50” E), is the closest hydrological station in the research area.

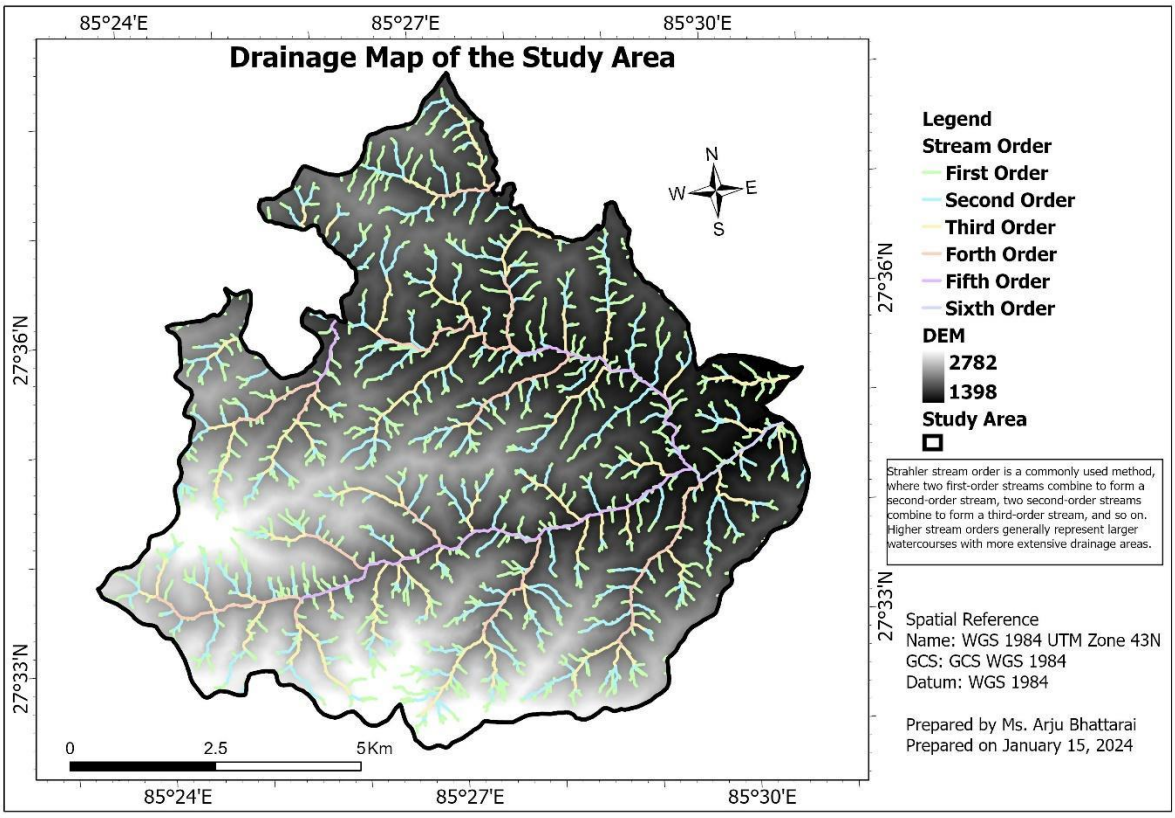

Figure 2: Drainage Map of the Study Area.

1.5 Problem Statement of the Study Area

Nepal, a landlocked nation in south Asia, is rapidly becoming an uncontrolled metropolitan area. Large and expanding infrastructure deficiencies as well as ineffective planning pose a threat to Nepal's urbanization's sustainability (World Bank 2013). The hilly region is prone to the formation of landslides with even small changes in geometry or burdening of unstable slopes, so the main cause of the landslide may have been caused by its geological structure and terrain morphology. Hilly region of Nepal is vulnerable to hazard because of steep terrain and rugged topography, making it highly susceptible to landslides. Rapid urbanization, deforestation, and erratic rainfall patterns further exacerbate the vulnerability of the region to landslides (Petley et al., 2007). In the rugged landscape of Kavre district, the rapid pace of urbanization intertwines with the intrinsic vulnerability to landslides, creating a precarious scenario for sustainable development. As urban areas expand and infrastructure deficiencies loom large, the specter of landslides casts a shadow over the region's future (Bhandari et al., 2015). Without robust planning measures and proactive strategies, the risk posed by landslides remains largely unaddressed, leaving communities vulnerable to potential disasters. The absence of comprehensive susceptibility mapping exacerbates this

vulnerability, hindering efforts to identify high-risk areas and implement targeted interventions. In this context, conducting a geospatial analysis to assess landslide susceptibility emerges as an imperative (Bera et al., 2019). By leveraging advanced technologies and analytical techniques, this research aims to unravel the complex interplay of geological, topographical, and anthropogenic factors shaping the landscape's susceptibility to landslides. The resulting insights hold the potential to inform evidence-based decision-making, empower stakeholders, and pave the way for sustainable urban planning in the Panauti area. The study area within the Panauti municipality is classified as a tourist area with parks, gardens, paragliding, and further infrastructure development underway. The registered landslide areas in the area are ward number 4, 8, 3, and 12 of the Panauti Municipality. In this situation, landslide susceptibility mapping is crucial because it identifies the area that is susceptible to landslides by ranging from low to high chances of a landslide occurring in the given area. The landslide susceptibility would serve as the foundation for the Panauti Municipality's future planning.

1.6 Research Questions

Landslide research aims to produce LSM using Hierarchical and Quantitative Method. This includes identifying the triggering mechanisms for landslides. The research findings will be combined with GIS modeling to provide a landslide susceptibility map for the area of interest. The study of this area aims to cover all the question listed below:

RQ1: What are the key factors influencing landslide susceptibility in Nagi Danda, Kushadevi in Panauti Municipality, and how can they be integrated to produce an accurate landslide susceptibility map?
RQ2: What portion of areas are covered by different level of susceptibility classes?
RQ3: What are the possible type of failure that makes the area landslide susceptible?

1.7 Objectives

1.7.1 Main Objectives

O1: To produce a landslide susceptibility map of the Nagi Danda, in Panauti Municipality using Geospatial Analysis, Quantitative and Hierarchical method. (RQ1 and RQ2)

1.7.2 Specific Objectives

SO1: To assess the existing bio physical conditions in relation to the landslide susceptibility mapping and categorization in different susceptible classes. (RQ2)

O3: To conduct Kinematic analysis in major landslides of the study area. (RQ3)

1.8 Limitations

There was no previous landslide inventory map in the study area which indicate no previous study about landslides were done in the area, resulting in difficulty in understanding Landslides causative factors. As a result, identifying landslide-prone areas has proven difficult. Fieldwork was conducted in wet season, hence the lithological exposure was covered in foliage, which disrupted the data collection procedure.

CHAPTER 2: Literature Review

2.1 Review in Landslide and Landslide Susceptibility mapping

Landslides, being one of the principal natural hazards, account annually for huge property loss in terms of both direct and indirect expenses. Landslides are defined as the movement of a mass of rock, debris or earth down a slope (Cruden & D.M., 1991). Landslides can move in one of several ways, including flowing, sliding, toppling, or falling. In general, landslides are caused by a combination of geo-environmental factors i.e. many landslides include two or more different movement types (Varnes & D.J., 1978). Landslides have frequently caused property and infrastructure damage and occasionally resulted in human losses. According to literature, between 1990 and 2005, landslides accounted for 5% of all natural hazards around the world. These numbers are likely to increase in the future as a result of seismic activities, climate change-induced rainfall levels, and human activity on fragile slopes (Kanungo et al., 2009). Landslides have caused large numbers of casualties and huge economic losses in mountainous areas of the world. The most disastrous landslides have claimed as many as 100,000 lives (Li et al., 1992).

The Varnes classification is a widely used system for categorizing landslides based on their type and the materials involved. It was first proposed by Varnes in 1978 and has since been adopted by many researchers and organizations. The classification takes into account the type of movement, the nature of the materials involved, and other relevant factors.
The main categories in the Varnes landslide classification include:

- **Falls:** Discrete masses of soil and rock falling through the air.
- **Slides:** Movement of material along a well-defined surface.
- **Flows:** Movement involving material that behaves as a viscous fluid.
- **Complex Movements:** Combinations of different types of landslides or those that don't fit precisely into the other categories.

Each of these main categories is further divided into subcategories based on specific characteristics of the landslide. The classification provides a systematic way to describe and categorize landslides, aiding in the understanding and management of landslide risks. Keep in mind that there might be updates or revisions to classification systems over time, so it's always good to check for the latest information from reputable sources (Cruden et al., 1996). The basic principle behind landslides is slope instability. Slope stability expresses a balanced

relationship between shear stress and shear strength (Duncan, 1996). Gravity-induced shear stress exists in every slope and increases with slope height, slope inclination, and the unit weight of the components that constitute the slope. Thermal expansion and contraction of surface zones, freezing-thawing activities, and other variables all contribute to increased shear stresses. Under typical conditions, slope surfaces are balanced between shear stress and shear resistance. A landslide can be caused by an imbalance of resisting and pushing forces (Duncan, 1996). Driving forces are those forces which move earth materials downslope. These include components of weight of material including fill material, vegetation, or buildings. Resisting forces are those forces which oppose the movement. These include strength of material. Factor of safety (FS): The factor of safety of a slope is the ratio of resisting forces to driving forces, i.e. FS = resisting forces / driving forces. The slope is stable if the driving forces are less than or equal to the resisting forces (i.e., when FS ≥ 1). However, when the driving forces exceeds the resisting (i.e., when FS < 1), the slope is unstable and a landslide may occur. Those parameters that increase shear stress and reduce shear strength of the slope could be categorized into external and internal factors including topographic parameters such as slope, ground water, soil moisture, lithology; geological structures such as faults, joints, bedding planes. Most common external factors influencing landslides are the vibrations due to earthquakes, blasting due to explosives and volcanic eruptions etc. Broadly, causes of landslides can be discussed under the following terms: geological factors, morphological factors and factors associated with human activity.

While semi-quantitative approaches rely on weighted techniques, qualitative strategies base their rating process entirely on indigenous knowledge (Abdo, 2022). On the other hand, quantitative approaches employ statistical methods to determine the connection between landslide beginning factors and landslide incidents (Rahman et al., 2022). Spatially landslide probability can be predicted using several quantitative methodologies, such as fuzzy logic (FL), logistic regression (LR), AHP, fuzzy neural network (FNN), the weight of evidence (WoE), information value (IV), fuzzy ratio, and fuzzy logic (Mohammady et al., 2012 ; Shahabi & Hashim, 2015). After earthquakes, landslides are the most frequent natural hazard in Turkey (Gokceoglu, 2002), with the Eastern Black Sea region being particularly vulnerable. The topography of this area is mountainous, and it frequently experiences high levels of precipitation. The combination makes the area vulnerable to widespread, catastrophic landslides. Natural disasters in Turkey over the past 50 years have resulted in housing losses

estimated. About US $80 million is lost economically each year as a result of landslides, with the Eastern Black Sea region bearing the brunt of these losses (Yalcin, 2007).

Similarly, in the context of Nepal's unique tectonic setting, high weathering rates and abundant rainfall, landslides are a major natural hazard. Human interference in the form of rapid urbanization and construction of infrastructure makes the situation even worse. In addition, landslide problems have worsened in Nepal and around the world as a result of climate changes and an increase in the frequency of extreme event (Siwakoti & D.R., 2000). According to the statistics, there is a significant degree of annual variability in the frequency of landslides, although general trends point to an increase. Landslides are a significant development impediment in Nepal, resulting in significant financial losses and a notable annual death toll. Everyone agrees that landslides are having more and more effects over time in nations like Nepal (Petley et al., 2007). Planning for land use requires an understanding of the slope instability's geographical distribution (Yalcin et al., 2011). Due to a complicated mix of factors including earthquakes, climate change, and an explosion in unofficial road building that destabilizes slopes during the rainy season, the number of landslide deaths in Nepal has been rising sharply. This tendency is expected to increase with further growth, particularly since China's Belt and Road Initiative aims to build three significant trunk highways across the Nepalese Himalaya, which nearby communities would try to connect to with shoddy roads (McAdoo et al., 2018).

2.2 Review related Geology of Central Lesser Himalaya Nepal

The Nepal Himalaya is the longest section of the Himalayas. It occupies the central position and extends all over the Nepal. The entire length of the Nepal Himalaya is over 800 km extending from the Mahakali River in the west to the Tista River in the east.

The Nepal Himalaya can be divided into five tectonic zones from south to north as proposed by Gansser, 1964 and Hagen, 1969 i.e.

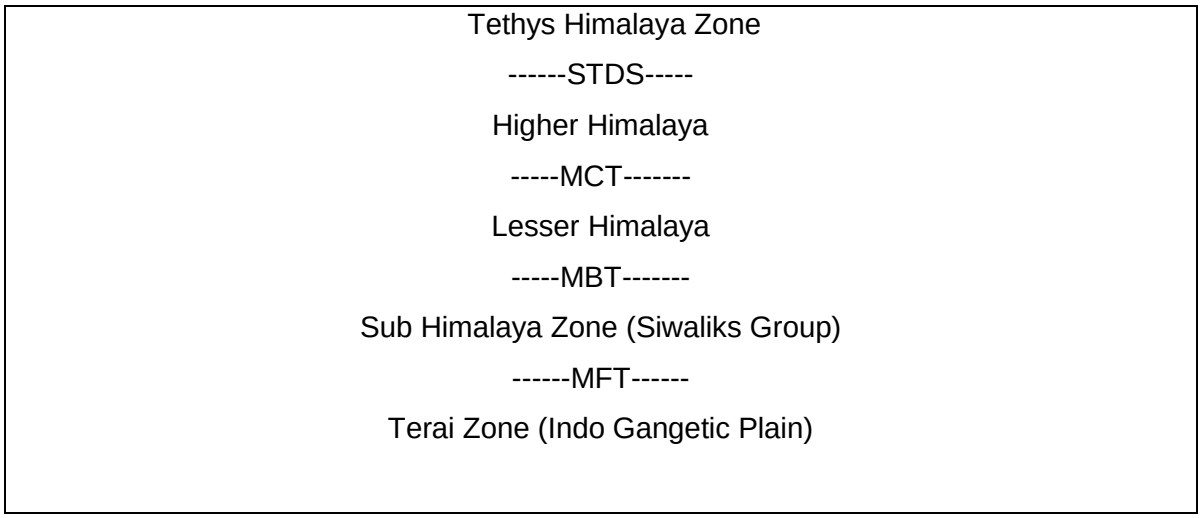

Figure 3: Division of Nepal Himalaya into 5 tectonic zone by Gansser, 1964 and Hagen, 1969

According to Stöcklin and Bhattarai (1977), the Kavre area's rocks can be classified into two types: crystalline high-grade metasedimentary rocks and Kathmandu Nappe (Complex). Similarly, while studying geology of Kavre area the Bhimphedi Group, divided by the Chak-Rosi Thrust, and the Benighted Slate of the Upper Nuwakot Group comprise the lithological units dispersed throughout the research region. The lithological units constitute the eastern closure of the NW-SE and dip southward. A portion of the Mahabharat synclinorium's northern limb. Psammitic schist, metasandstone, metasiltstone, and micaceous quartzite make up the majority of the geology in the area. One type of rock found in the Markhu, Kalitar, and Chisapani formations is micaceous quartzite. Markhu quartzite has a minor calcareous content. One type of rock found in the Kulekhani and Markhu Formations is pazmitic schist. The Tistung Formation's two main rock types are metasandstone and metasiltstone. The primary joint sets in the rock masses are three to four, including the joint parallel to foliation. The discontinuity characteristics show that the rocks have a virtually smooth to rough surface with soft filling aperture, indicating that they are blocky in nature. The rock bulk is rigid, indurated, and almost entirely new. Toppling failures, plane failures, and stable and unstable wedges all affect the slopes (Paudel & Tamrakar, 2013).

The primary causes of large-scale landslides on central Nepal's highways are the significant hydrothermal alteration in the Lesser Himalaya during the Main Central Thrust (MCT) and, consequently, clay mineralization in sliding zones of large-scale landslides. Additionally, this study indicates that slope failure in the Lesser Himalaya of Nepal during the monsoon is primarily caused by large-scale landslides (Hasegawa et al., 2009).

The local tectonic activity has caused these rocks to fracture and fold. The region's tectonic activity has resulted in folding and faulting. Sedimentary rocks, such as sandstones,

siltstones, and shales, were deposited during the Jurassic and Cretaceous periods. Metamorphic rocks, such as gneisses, granites, and schists, are products of the intense heat and pressure that go into the development of mountains (Stöcklin & Bhattarai, 1977) The area is prone to landslides and rock falls because of the steep terrain and deteriorating rocks. In 2014, there was a landslide in the nearby Sindhupalchowk area that caused substantial damage and killed several people (Geest & Schindler, 2016). In conclusion, Kushadevi's geology has been formed by tectonic activity associated with the Himalayan Mountain.

2.3 Review on LSM using various methods

A section of the Himalayan region near Darjeeling was chosen for the model's execution. The area is divided into various zones of four relative susceptibility classes: high, moderate, low, and very low, on the resulting landslide susceptibility map. The validation of the susceptibility map involved a correlation between the frequencies of landslides in various classifications (Sarkar & Kanungo, 2004). In Dena city, Iran, susceptibility maps are created using the AHP in eight layers accordingly, landslide inventory, rain, lithology-weathering, earthquake, slope, land cover, distance to stream, and distance to road. This method divides each layer into smaller components, weights these components according to their significance, then assembles the last set of prepared layers and creates the final map which gives a satisfactory result. Since historical landslide databases provide the foundation for all landslide risk assessment components, their availability and quality cannot be overstated. In contrary the Namche area of the South Sikkim district, which is a part of the Eastern Himalayas. The multi-criteria analysis technique was used to map the zonation of landslides hazards. A GIS platform (ArcGIS 10.1) was utilized to combine multiple thematic layers, including slope, rainfall distribution map, lineament density, drainage density, slope aspect, geomorphology, land use/land cover, and soil map, in order to demarcate the landslide hazard zone (Bera et al., 2019). GIS and remote communications are examples of modern technology that ought to be used more often in landslide risk assessment and management (Moradi et al., 2012). Risk assessment is necessary to make wise decisions and funding for landslide management. The historic landslide database cannot be over emphasized as it contains all the basic components for landslide risk assessment which leads to its management (Dai et al., 2002). In order to manage disasters and plan land use, it is crucial to identify and map locations where landslides are likely to occur. This goal can be effectively accomplished by using landslide susceptibility prediction, or LSP (Borrelli et al., 2018).

Geographic Information System (GIS) technology has been widely employed in recent years for mapping and assessing the susceptibility to landslides. It is often integrated with data obtained through novel approaches, such as satellite remote sensing and light detection and ranging (LiDAR) photographs. GIS-based models make it possible to manage large amounts of data in terms of file size and geographic scale. They also enable the dynamic and ongoing zonation of landslide susceptibility, which is a necessary step in efficient land planning and risk reduction (Yalcin et al., 2011). The GIS-based approach that has been suggested to map the susceptibility to landslides in the Portofino promontory, a Mediterranean region that is occasionally impacted by severe rain events that result in frequently shallow landslides, is one of the research that this study will look at. Drawing on more than 110 years of landslides nine landslide conditioning factors, including both natural and anthropogenic aspects, have been evaluated for their role using a semi-quantitative AHP method based on inventory and expert judgments (Roccati et al., 2021). The AHP method is one of the heuristic methodologies that has been used extensively in the literature for landslide susceptibility assessments. AHP is a multi-criteria approach that is widely utilized in natural hazard management because of its ability to link physically diverse data (Yalcin, 2008). According to comparatively higher or lower probability or categories of probabilities, susceptibility mapping identifies areas within the research area that are more or less vulnerable to landslide (Tehrany et al., 2015). Through the identification of landslide-prone zones (high to low), the LSM will assist stakeholders in putting suitable mitigation measures in place throughout the rural municipality affected by landslides (Dhungana et al., 2023). The class FR or class weights, which show the relative relevance of distinct classes for each factor, were derived using the FR model. The landslide susceptibility index value (LSIV) on a GIS platform was calculated using the weighted linear combination (WLC) approach, which takes into account both factor weights and class weights. There are five zones within the Shiv-khola watershed that are susceptible to landslides (Mondal & Maiti, 2013).

The Dakar coastline region was subjected to a multi-method approach for mapping landslide hazards and evaluating the stability of natural slopes. This method is based on the successful fusion of GIS, mechanical (deterministic and numerical) stability analysis, and geotechnical field and laboratory work. This method produced useful findings about slope failure modeling, landslide kinematics, instability factors, and coastal erosion. This resulted in an extensive evaluation, a significant decrease in the subjectivity of the slope stability and hazard assessment, and the creation of an objective map showing the threat of landslides along Dakar's southwest shore (Fall et al., 2006). Slope stability analysis is used for study of slopes,

whether man-made or natural, and the state of equilibrium. The resistance of an inclined surface to collapsing or sliding is known as its slope. Property and lives loss may result from a slope failing. Therefore, it is crucial to verify that the suggested slopes are stable. With the advancement of contemporary soil testing and stability analysis techniques, a cost-effective and secure slope design has been made possible (Salunkhe et al., 2017). The kinematics of past landslides in an area, geologists and engineers can create hazard maps that delineate zones prone to landslide activity. These maps serve as valuable tools for land-use planning, infrastructure design, and emergency preparedness (Rusydy et al., 2019). Furthermore, the incompleteness of the input variables in LSP modeling results from the ignoring of the variety of conditioning factors in slope units. The internal variations of conditioning factors within a slope unit, which are represented by the descriptive statistics features of mean, standard deviation, and range, are used in this study to construct LSP modeling from the slope units extracted by the MSS method (Chang et al., 2023). As a result, the rockslide at Theng has been thoroughly examined at 24 different sites utilizing topographic, lithological, and structural data gathered from the ground. The goal is to assess the causes underlying rock sliding in order to provide the best mitigation strategy. This study's large-scale geological mapping and site-specific kinematic analyses in various spatial domains confirmed that, despite the competent lithology (quartz, gneiss, and quartzite) within this 180-meter stretch, there is a high likelihood of both plane and wedge failures due to gentler and unfavorably oriented planar discontinuities with respect to the available resources (Ghosh et al., 2014). The study in the East Sikkim Himalaya evaluates landslide susceptibility maps (LSM) using frequency ratio, logistic regression, random forest, and integrated analytical hierarchy process with frequency ratio (AHP-FR). Models trained with 166 landslides and 12 causative factors were tested against 71 landslides, revealing very high susceptibility classes covering 11.97% for AHP-FR, 11.99% for logistic regression, and 7.13% for frequency ratio, with random forest and AHP-FR showing superior performance based on success rate curve, prediction rate curve, and seed calculation area index metrics (Gupta et al., 2022).

CHAPTER 3: Materials and Methodology

For the purpose of geological mapping and landslide investigation, the study work was conducted mainly into three stages viz.

- Desk study
- Field study
- Data analysis interpretation and presentation

3.1 Data Used

Spatial datasets play a pivotal role in advancing the accuracy and efficacy of landslide susceptibility mapping through the integration of the AHP method and the FR method. In the AHP method, spatial data sets are instrumental in delineating criteria such as slope, land cover, and lithology, which are crucial factors influencing landslide occurrences. These datasets enable the quantification of pairwise comparisons and the assignment of weights to each criterion, providing a geospatial foundation for decision-makers (Saaty et al., 2001).

Similarly, in the FR method, spatial datasets are fundamental for identifying conditioning factors associated with landslide occurrences. Features like slope, land cover types, and lithological characteristics are spatially represented, forming the basis for calculating the frequency of landslides within specific classes. The spatial mapping of landslide frequency outcomes assists in visualizing areas at higher risk. Integrating spatial data into the FR method enhances the precision of susceptibility mapping by considering the spatial distribution of conditioning factors, providing a more accurate assessment of landslide susceptibility across diverse landscapes. The synergy between spatial datasets and both AHP and FR methods fosters a comprehensive understanding of landslide susceptibility, thereby supporting informed decision-making and proactive measures for landslide risk mitigation and management (Mondal & Maiti, 2013). ASTER DEM was used for the extraction of topographic attributes namely slope, aspect, drainage, curvature, topographic wetness index (TWI). Sentinel 2 level 2 high resolution image of 2024 February was used for LULC map preparation. Similarly, for average precipitation map (2010-2022) CSV data file was used. Similarly, for fault and lithology Vector data sets from DMG was used.

The different data used in this investigation are listed in Table 2.

Table 2: Datasets used, its Description, Source and Type.

Data	Description	Source	Type
Landslide inventory (Point and Polygon)	Point/ Polygon	Google Earth And Field verification	Vector
Kinematic analysis (Jointset data)	Point	Field Work	Vector
Slope, Aspect, Curvature, Stream Network, TWI Index	Will be derived from DEM	ALOSPALSAR|Alaska Satellite Facility	Raster
Geology (Lithology)	Geological map of Nepal prepared by ICIMOD by using geological Map of 1 : 100000 scale published by Department of Mines and Geology in 1994.	Data from mines and geology Department	Vector
Distance from stream network road network and fault	Euclidean distance function will be used for calculating the distance from the Stream Network, and Fault distance	Dem data from Alospalsar for stream distance, Nepal road network - Humanitarian Data Exchange (humdata.org) for road distance and geological map from department of mines and geology, lazimpath	Raster/Vector

Precipitation	Monthly average rainfall data from Metrology Department	Meteorological department	Raster
LULC	Land used land cover	Esri | Sentinel-2 Land Cover Explorer (arcgis.com)	Raster

3.1.1 Grid Size and Coordinate System Projection Used:

In this research, all datasets required for the study area were kept to a resolution of 12.5 meters. The DEM and its derivatives, distance raster datasets, geology, precipitation, and landslide inventory polygon files were resampled to 12.5 m resolution using ArcGIS Pro's resampling tool.

3.1.3 Image Processing

Before compositing and mosaicking, Sentinel-2 Level-2A bands were reduced to the area of interest, resampled to 12.5 m pixels using ArcGIS pro, and saved in ENVI format. Resampled images were composited into a single image using ArcGIS Pro software. Next, the composited band picture from the preceding procedure was utilized to mosaic two image layers into a single continuous image. Two DEM Image layers were overlaid to provide continuous DEM images for the study region.

3.1.4 Data Processing

- Clipping and Masking is the process of pulling data from a specified area of interest. The clip function aligns the scope of one geographical layer with another. All datasets in this study were cut to cover a larger study area.
- Rasterization is the process of turning vector data (points, lines, and polygons) into raster form (pixels). The polyline and polygon conversion tool is essential for converting these data types to raster. In the present The Landslide factors and

Landslides files were rasterized using the polygon to raster tool, with a cell size of 12.5m.

- The raster object is created through resampling, which adjusts the spatial resolution of the input raster by developing rules for aggregating or interpolating data over new pixel sizes. This study resampled DEM datasets using closest neighbor resampling, with output cell size set to Sentinel 2 Level 2A (12.5 m). The fastest interpolation technique is nearest neighbor, which preserves cell beginning values and is suitable for discontinuous data such as land use classification (ESRI, 2021).

  The Spatial Analyst toolbox and is used for reclassifying raster data. This tool allows users to modify the values of a raster dataset based on specified ranges or criteria.

For the Landslide susceptibility mapping total 10 factor are used after reading multiple paper, field work i.e. Slope, Slope Aspect, Curvature, Stream, Road, Rainfall, Lithology, TWI, LULC and Distance from fault.

3.2 Software used:

There are various range of software to be used for landslide susceptibility mapping and they are as follows:

Table 3: The software used with its purpose.

S. No.	Software Used	Purposes
1	ArcGIS Pro 10.4	For data analysis
2	Google Earth Pro	To create landslide inventory map
3	Google Maps	To trace the location of landslide
4	Geojson.io	To trace the GPS and code it to shape file
5	DIPS	For Kinematic analysis from the field data

3.3 Desk study

Various published and unpublished reports regarding the geology of the study area were studied as mentioned in Chapter two. The material used for the desk study is topographic map of 1:25000 scales. Google earth images had also been used during the study. Land use map and the digital elevation model (DEM) were derived from the digital data provided by Survey Department. Precipitation data were obtained from Department of Hydrology and Metrology.

3.4 Field study

Desk study was followed by a series of detailed fieldwork in the study area. About 2 weeks were spent in the different time periods for the data collection. The fieldwork was performed with the aim of preparing the geological map and the landslide inventory map of the study area. Brunton compass, topographic maps, geological hammer, magnifying glass, measuring tape, hydrochloric acid and graph papers were used for the field study.

The Geological structure like fold and fault were also marked on the map.

The landslides observed during the field study were marked on the map to prepare up to date landslide inventory map. To study the geology from the Geology of Nepal Himalaya by Prakash Das Ulak and study the geomorphology of that area presence of fault, fold, lithology and its contribution in landslide.

3.5 Landslide Inventory mapping:

For this purpose, Google Earth Pro is to be used to digitize the landslide on going area and to confirm the landslide area fieldwork will be performed. The data will be classified into training data for creating LSM and testing data for validation of LSM. The Tabulate Area tool in ArcGIS Pro was used to calculate the number of landslides area and their corresponding pixels across various parameters. The landslide point and polygon datasets were converted to raster format using the conversion tool.

Landslide susceptibility mapping involves predicting the likelihood of landslides occurring in a given area based on various factors. To create accurate and reliable models, it's crucial to have well-prepared training and testing datasets as given in Table 4.

Table 4: Division of landslide point datasets.

Datasets	**Division of datasets**	**Purpose**
Training Set	70% of total dataset	Used to train the landslide susceptibility model
Testing Set	30% of total dataset	Used to assess the model's performance and generalization

3.6 Slope Stability Analysis Using DIPS:

For the kinematic analysis of slope failure data were collected from joints of exposure of landslide in the field and the failure analysis is done using DIPS software. Gather geological

and geotechnical data related to the slope. This includes information on joint orientations, spacing, persistence, roughness, and any other relevant geological features.
The joint orientation data (dip and dip direction) into DIPS. This data is typically collected in the field using a compass. To calculate the failure; joint datasets (joints having similar orientations) area collected. The field data are given as input data to dips and it analyze the data giving the failure percentage.

3.7 Data analysis:

Landslide susceptibility mapping and analysis need consideration of multiple factors. Total 10 factors are used for the preparation of LSM of the study area through studying various literature and interviewing locals and conducting rigorous research to investigate landslide sites. During the 15 days of fieldwork in August 2023, landslide areas were GPS-identified. The LSM was prepared by considering ten landslide triggering factors: lithology, slope angle, drainage, slope aspect, slope curvature, lithology, fault, drainage, land use and land cover (LULC), Topographic Wetness Index, and precipitation.

3.7.1 Slope:

Slope stability calculations rely heavily on the slope angle, as it directly affects shear pressures. Sliding is more likely on steeper slopes. In most research on landslide sensibility zoning, slope % is one of the most relevant variables (Abedini et al., 2017). Theoretically, raising the slope increases shear stress, which increases the possibility for slope instability. The slope map of the research region is produced into five classes i.e. 0-15,15-30,30-45,45-6-, 60<. The slope map was derived from ALOS PALSAR DEM of 12.5 m resolution by using ArcGIS Pro software.

3.7.2 Slope Aspect

Slope Aspect element plays a vital part in utilizing the quantity of rainfall, solar energy, and type of wind blowing in any location, as well as reflecting the influence of soil thickness, vegetation, wetness, and so on. Because the research region is in the middle attitude, the susceptibility of landslides varies along the entire slope direction. The aspect map of the study area is created in nine classes. The aspect is defined as the angle formed by the steepest slope on the ground surface (Dahal, 2014). The slope direction is measured in degrees from

0° to 360° clockwise, with 0°, 90°, 180°, and 270° signifying slopes to the north, east, south, and west, respectively. According to (Dai et al. 2001), factors such as sunlight exposure, rainfall, drying breezes, and discontinuities can cause Aspect affect the stability of terrain surfaces by regulating soil moisture and vegetation growth based on the quantity of sunshine received (Dahal, 2014). This work used ArcGIS Pro to extract slope aspects from ALOS PALSAR DEM and categorize them.

3.7.3 Lithology:

Geology and geomorphology are important factors in landslide activity and susceptibility because different geological and geomorphological units have varying strengths and susceptibilities to landslides (Panchauri & Pant, 1992). The lithological stratigraphy was categorized into 6 formations after studying Nepal Geology Book and data from Department of mines and Geology. Extract by Mask tool was used to generate the lithology of study area and then digitized to specific category.

3.7.4 Distance from Road

Another aspect that influences landslide incidents is the distance to the road. Landslides have a strong correlation with it. Opening new routes and expanding existing roads can disrupt the natural morphology and undermine slope stability. During road building, continuous vehicle movement and variations in slope stability might lead to instability (Yalcin et al., 2011). Slope cutting cracks absorb a lot of water, leading to soil oversaturation and sloppy land slide. The study created a distance raster map using ArcGIS Pro's Euclidean distance analysis tool. Road distance rasters were grouped into three classes.

3.7.5 Distance from Fault

Thrust and fault are weak planes through which the tectonic movements occur. Due to the tectonic movements, the surrounding areas are highly fractured, faulted and weathered (Dahal, 2014). On such heavily crushed and weathered terrain, extreme rainfall can easily induce landslides Thrust and fault are weak planes through which the tectonic movements occur. Due to the tectonic movements, the surrounding areas are highly fractured, faulted and weathered. On such heavily crushed and weathered terrain, extreme rainfall can easily induce

landslide (Dahal, 2014).The fault zone was digitized reading various books and data sets from DMG. The resulting distance was determined map was divided into 3 classes.

3.7.6 Distance from Drainage

Another geomorphology-related causal element was the landslide's placement away from the stream, the location of the landslide from the stream was a geomorphology-related element. Field observations showed that slope groundwater migration and toe undercutting led to increased failure rates along the stream. A distance to drainage map was created to analyze landslide activity and determine susceptibility (Dahal, 2014). Field observations revealed that slope failure occurred more frequently along the stream due to groundwater flow towards the stream and toe undercutting. As a result, a distance to drainage map was created for landslide activity analysis and susceptibility assessment. To create the stream proximity map for susceptibility assessment, the drainage segment map was rasterized and the distance to the drainage was determined in meters. The resulting map was divided into 3 classes.

3.7.7 Land Used Land Cover

The Sentinel-2 Level-2A will be subset to the area of interest and resampled to the pixel of 10m, then stored in ENVI file format. Then, using ArcGIS Pro software, resampled imageries will be used for the Compositing band to generate a single image. The two image layers will then be mosaicked to create a single continuous image using the composited band image created using the preceding procedure. Supervised classification method will be used where Maximum likelihood will be used as classifier algorithm for Classification of Image (Esaid et al., 2018). The overall class accuracy will be evaluated using the Kappa statistics, which provides a statistically accurate assessment of the quality of classification (Esaid et al., 2018). In the study area LULC was classified into 5 classes.

3.7.7.1 Accuracy Assessment of Land Use Land Cover

I utilized 300 randomly selected sites and a stratified random sample method to assess product correctness. ArcGIS Pro software was used to test the accuracy of categorized images resulting from supervised classification, including determining the confusion matrix. High-quality satellite photos were interpreted visually to provide ground truth information. The assessment tools developed an error matrix that identifies users, producers, overall accuracy,

and Kappa accuracy level. Kappa statistics were used to test categorization accuracy (Esaid et al., 2018).

3.7.8 Precipitation

Rainfall is an important extrinsic variable for susceptibility analysis. Statistical landslide susceptibility study often uses regionally distributed average annual rainfall (Dahal, 2014). For the preparation of Precipitation Map Average monthly precipitation data from 2010 to 2022 of nearest six locations was used from Department of Metrology in CSV. File format. Then using Arc GIS pro and using Interpolation Tool Precipitation Map was created and divided into five classes.

3.7.9 Curvature

Slope curvature refers to the slope's curved shape. It greatly impacts the direction and aspect that influences landslide incidents is the distance to the road. Landslides have a strong correlation with it. Opening new routes and expanding existing roads can disrupt the natural morphology and undermine slope stability. During road building, continuous vehicle movement and variations in slope stability might lead to instability (Yalcin et al., 2011). Slope cutting cracks absorb a lot of water, leading to soil oversaturation and sloppy land slide.

3.7.10 Topographic Wetness Index (TWI)

TWI values from DEM are commonly employed as a proxy for soil moisture, as they impact both soil moisture and species (Kopecký et al., 2021). TWI takes into account both the catchment area and slope grade. According to Kumar and Anbalagan (2016), this phenomenon is linked to the accumulation of flow in specific terrains. TWI categorizes biological processes such as vegetation patterns, forest site quality, and yearly net primary output (Sorenson et al., 2006). Flat, convergent terrains have a greater moisture index than steep, divergent terrains. Soil moisture affects slope stability, particularly for landslides.

To calculate

The formula used:

TWI= ln(CA/tan slp) where CA represents catchment area and slp is the slope gradient. The TWI map for this study was built using ArcGIS Pro's raster calculator feature, starting with

a DEM and applying the aforementioned connection. The research area's TWI was divided into four classes.

3.8 Landslide Susceptibility Mapping

The study created a Landslide Susceptibility Index map for the research area using AHP and FR methods for comparison.

3.8.1 Analytical Hierarchical method:

The Analytic Hierarchical Process (AHP) is a systematic and structured decision-making method that has found application in landslide susceptibility mapping. AHP involves the decomposition of a complex decision problem into a hierarchy of criteria and alternatives, allowing for a comprehensive and organized assessment. In landslide susceptibility mapping, various factors such as slope, land cover, soil type, and precipitation contribute to the overall vulnerability of an area to landslides (Mondal & Maiti, 2013). AHP helps in assigning weights to these factors based on their relative importance, as perceived by experts or stakeholders. By pairwise comparisons, decision-makers can establish the priority of each criterion in influencing landslide susceptibility. Subsequently, these weights are used to calculate a composite susceptibility index for each location, providing a quantitative measure of its predisposition to landslides.

AHP not only facilitates the integration of diverse and subjective data but also allows for the incorporation of expert knowledge into the decision-making process. The method aids in producing more accurate and robust landslide susceptibility maps by systematically considering multiple factors and their interactions, enhancing the effectiveness of risk assessment and management strategies in landslide-prone areas. Weight for each factor to be assigned AHP depending on its influence on the landslide occurrence. The landslide susceptibility map was derived using weighted overlay method and categorized into five susceptible classes namely, very low (VL), low (L), moderate (M), high (H) (Kumar & Anbalagan, 2016).

This method is solved by developing pairwise comparison matrix (Table 3) by assigning the rank to each factor against other factors. Assigning rank using Table 4 based on degree of preference of factors influencing landslide. It depends on the weightage given by expertise in this research the possible weightage is given by studying multiple literatures, field work and consultation with expertise.

Table 5: Matrix of pairwise comparison (Saaty, 2000)

C	A1	A2	…	An
A1	a11	a12	…	a1n
A2	a21	a22	…	a2n
:	:	:	…	:
Am	am1	am2	…	amn

Table 6: The basic scale of preference between two variables for pairwise comparison matrix in AHP method (Saaty et al., 2001).

Importance Rank	**Degree of Preference**	**Explanation**
1	Equal importance	Both criteria contribute equally to the objective.
3	Moderately importance of one over another	Judgment and experience tend to prefer one criterion over another.
5	Strongly importance	Judgment and experience effectively favor one criteria over the other.
7	Very strongly importance	Experience and judgement take precedence over other factors, as evidenced by practice.
9	Extremely importance	The evidence supporting one criteria over another is the maximum degree of probability of an affirmation.
2, 4, 6, and 8	Intermediate values between two adjacent judgements	Used to represent compromising between the preferences in weights 1,3, 5, 7 and 9
Reciprocals	Opposites	Used for inverse comparison

In this model, the consistency index, also known as the ratio of consistency (CR), represents the likelihood that the matrix judgments were created at random. For LSM employing AHP, a consistency ratio of less than 10% is considered legitimate.

$CR = CI / RI$ *{Equation 1}*

Here RI stands for random index

Whereas CI is calculated by given formula:

$CI = (\lambda max - n) / (n - 1)$ *{Equation 2}*

Where, λmax is the principal or largest equivalence value of the matrix and could be calculated easily from the matrix and n is the matrix number (Saaty et al., 2001).

3.8.2 Landslide Susceptibility Index from AHP Method:

The weighting/rating values for all contributing factors and factors' classes were calculated in AHP Excel sheet. From the literature review, the general equation for creating LSI map is shown below (Saha et al., 2002; Pokharel & Thapa, 2019; Kumar & Anbalagan, 2016)

LSI= $\sum n\ i=1\ Ri * Wi$ *{Equation 3}* Where,

LSI= Landslide Susceptibility Index

Ri= Rating class of each layer.

Wi= Weights of each landslide causative factors. In this research, equation3 formula was applied in for generating LSI map by using weighted overlay function available in ArcGIS Pro. Later on the susceptible classes was divided into 5 different classes i.e. Very High, High, Moderate, Low, Very Low (Hasekioğulları & Ercanoglu, 2012).

3.8.3 Frequency Ratio Model:

The Frequency Ratio (FR) method is a statistical technique commonly employed in landslide susceptibility mapping. This method relies on analyzing the spatial distribution of landslides in relation to different conditioning factors to assess the likelihood of future landslide occurrences. The key premise behind the Frequency Ratio method is that certain environmental variables or factors contribute more significantly to landslide susceptibility.

To apply the Frequency Ratio method, various conditioning factors such as slope, land cover, lithology, and rainfall are considered. The process involves calculating the ratio of the frequency of landslides within a specific class of each factor to the overall frequency of landslides in the study area. The resulting ratios provide a measure of the relative importance of each factor in influencing landslide occurrence. For instance, if areas with a certain slope range experience landslide more frequently compared to the overall average, the Frequency Ratio for that slope class would be greater than 1, indicating a higher susceptibility. Conversely, a Frequency Ratio less than 1 implies a lower susceptibility (Ehret et al. 2010).

By combining the individual Frequency Ratios for each factor, a composite landslide susceptibility map is generated. This map categorizes different areas based on their susceptibility to landslides, providing valuable information for land-use planning, risk assessment, and disaster management. The Frequency Ratio method is particularly useful in

areas where historical landslide data is available and can be used to identify and prioritize areas at higher risk of landslides**.**

Frequency Ratio (FR) is one of the bi-variate statistical approaches of landslide susceptibility assessment which is based on observed relationships between landslide distribution and each causative factor related to landslides. This technique can be used to determine the spatial correlation between the site of landslides and the explanatory elements for them (Yalcin et al., 2011). Based on their association with the occurrence of landslides, the FR for each subclass of individual causative factor is determined. The frequency of sub-class of each causative factor can be calculated by using the following formula (Ehret et al. 2010).

Frequency Ratio= (Mi/M) / (Ni/N) *{Equation 4}*

Where,

Mi= Number of pixels with landslides for each subclass conditioning factor, M= Total number of landslides pixels in the study area,

Ni= Number of pixels in the subclass area of each factor and N=Total number of pixels in the study area (Ehret et al. 2010).

3.8.4 Landslide Susceptibility Index from Frequency Method

The Landslide Susceptibility Index was computed by adding up the raster datasets generated from the application of frequency ratio based on equation (4).

LSI= Fr1+Fr2+Fr3+….+Frn *{Equation 5}*

Where, LSI= Landslide Susceptibility Index, Fr= Rating of each factor's class.

After that using Raster Calculator tool in ArcGIS Pro was used to generate the landslide susceptibility Index. LSI map into 5 various landslide susceptibility categories, including very low, low, moderate, high, and very high (El Jazouli et al., 2019).

3.8.5 Validation:

The Roc (Receiver Operating Characteristic) curve is a valuable tool in the field of landslide susceptibility mapping, providing a quantitative assessment of the model's performance in predicting landslide occurrence. This curve helps in identifying the balance between correctly predicting landslide occurrences and minimizing false alarms. Researchers can use the Roc curve to determine the reliability of the susceptibility model, refine parameter settings, and enhance the overall accuracy of predictions. Therefore, the Roc curve serves as a crucial tool in guiding the development and validation of landslide susceptibility mapping models,

contributing to more effective and reliable hazard assessment and mitigation strategies (Hoo et al., 2017).

For evaluating model accuracy, a variety of statistical techniques are available, including error rate, ROC (Receiver Operating Characteristics) plot, success rate curve, and prediction rate curve. In the present study, the accuracy of the landslide susceptibility map will be validated by using success rate curve technique (Kumar & Anbalagan, 2016). The ROC curve is a popular validation technique, however it only measures the overall reliability of geographical prediction maps and does not account for spatial pattern uncertainty. To decrease conflicts and build a reliable map, all LSMs were merged with overlaying statistical methods to determine the best zone pattern from overlapped patterns (Vakhshoori & Zare, 2018). The Table 7 gives categorization of ROC curve on the basis of value obtained.

Table 7: The categorization of ROC Curve Value.

AU-ROC Curve Value	**Category**
0.9-1.0	Excellent
0.8-0.9	Very Good
0.8-0.7	Good
0.7-0.6	Satisfactory
0.6-0.5	Poor

3.9 Methodological Frame Work of the Study area

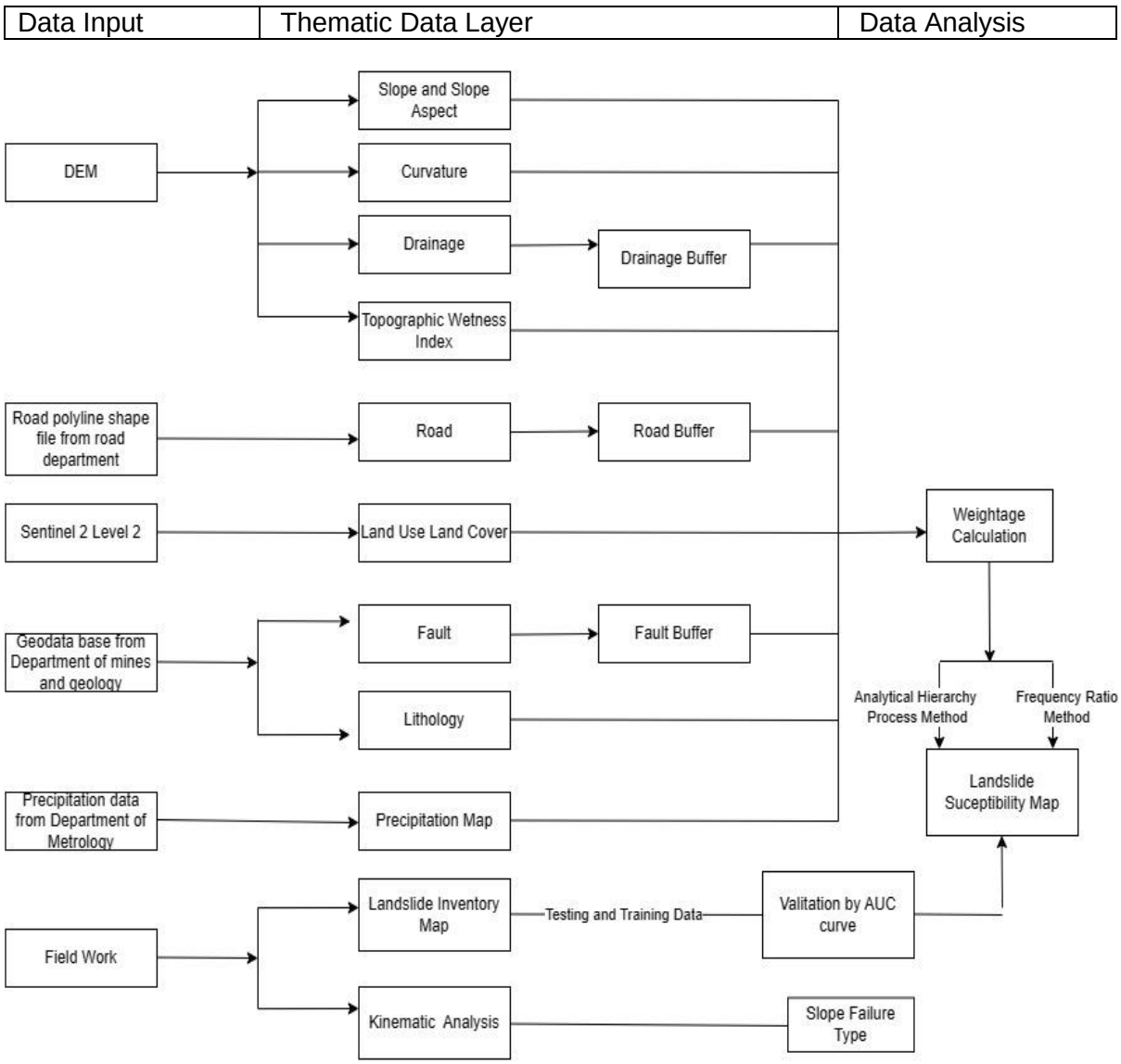

Figure 4: Methodological Frame Work of the Study Area

CHAPTER 4: Results

4.1 Litho stratigraphy of the study area:

The study area is covered by the rock succession of low-grade metamorphic equivalent of the Precambrian Devonian, Phulchauki Sub Group of the Lesser Himalaya. All the five formation i.e. Pulchauki Formation, Chitlang Formation, Chandragiri Formation, Sopyang Formation and Tistung Formation is found in study area. The primary lithology of the area is fine clastic sequence of metasandstone, siltstone, phyllite, shale in tistung formation, the overlying sopyang formation is transitional phase between the fine grained classic Tistung and the thick young Chandragiri limestone. The Chandragiri limestone is the distinct formation of Pulchauki group due to thick lime stone sequence similarly Chitlang formation consists of dark purplish soft weathered slates. Godawari or Pulchauki formation is the youngest formation in Kathmandu Nappe itself which consists of medium to coarse grained massive crystalline limestone and dolomite to grayish blue purplish color (Stocklin and Bhattarai, 1977) . The major geological structure seen in this area s fold, fold and faults.

4.1.1 Faults:

A fault is a fracture or zone of fractures in the Earth's crust along which movement has occurred. These movements can be horizontal, vertical, or oblique, and they are typically a result of tectonic forces acting on the Earth's lithosphere. Faults play a crucial role in the deformation of the Earth's crust and are responsible for earthquakes. The previous studies indicate multiple fault in this reason however, it was not clearly seen in the field work.

4.1.2 S fold:

"S-type fold" typically refers to a type of folding structure in geology. Folding is a common geological process where rock layers deform due to tectonic forces, leading to the creation of folds. S-type folds are characterized by their sinusoidal or serpentine shape, resembling the letter "S" as shown in photograph 1. S-type folds are often associated with compressional tectonic forces. These forces cause the Earth's crust to deform, resulting in the folding of rock layers. The exact geometry of the fold depends on factors such as the type of rocks involved, the intensity of tectonic forces, and the temperature and pressure conditions.

Photograph 1: S-type fold observed in field work near Roshi Khola area

4.1.3 Fold:

In geology, a fold refers to a bending or deformation of rock layers that results from tectonic forces acting on the Earth's crust. Folding is a common geological process that occurs over long periods due to compressional or extensional stress. The resulting structures, known as folds, provide important insights into the tectonic history and geological evolution of a region. Multiple folds were observed during the field work as shown in Photograph 2.

Photograph 2: Fold observed during fieldwork up to the Nagidada hill.

.

4.2 Landslide Investigation

Throughout the field investigation, a variety of mass movements were noted and mapped out throughout the area. In the research region, there are several types of mass movement, including complicated, debris, and earth slides. Less time and effort was put into the in-depth categorization and analysis of landslides because the primary focus of the study was on their detection and demarcation. Therefore, the current study does not incorporate all relevant information on the types, histories, and potential causes of landslides. Here, a brief attempt is made to describe a handful of the area's most significant mass movements. All together 138 landslides were observed in the field.

4.2.1 Debris flow

A debris flow is a type of mass wasting or mass movement that involves the downhill movement of a mixture of soil, rock, and other debris. It is a fast-moving, gravity-driven flow that can occur in mountainous or hilly terrain, especially in areas with steep slopes. Debris flows are often triggered by heavy rainfall or any other factors that saturate the ground and mobilize loose materials. Multiple debris flow was observed during the field visit among them debris fall just below the altitude of Nagi hill at spatial extent 27°34'41.66"N and 85°27'32.59"E is observed which is shown in Photograph 3. This also show a failure of gabion wall hence other bioengineering mitigating measures could be a mitigating measure.

Photograph 3: Debris flow at Nagi dada showing failure of mitigation measure

Similarly, another location near to Nagi uphill another landslide was observed due to road cutting is observed in below photograph 4. The instability was caused by the toe cutting during the road construction.

Photograph 4: Landslide due to road cutting in the study area.

4.2.2 Rock fall

Rock falls are events where rocks or rock fragments detach from a steep slope or cliff and fall to the ground below. They are often triggered by various factors, including weathering, freeze-thaw cycles, seismic activity, and human activities. Rock falls can pose serious hazards to people, structures, and transportation routes in mountainous or rocky terrain.

Near to the Roshi Khola on the way to the Nagi hill major chances of rock fall was seen due to the unplanned mining work as shown in Photograph 5.

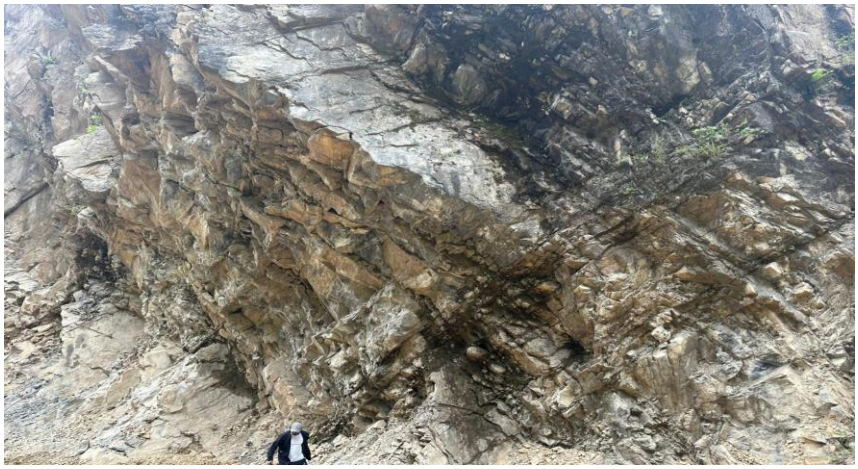

Photograph 5: Rock fall chances in the mining sites near Roshi Khola.

4.2.3 Kinematics analysis

For kinematics analysis, three major area of landslide is taken from each landslide 50 to 60 data is collected using Brunton Compass and the DIPS Software is used which provide us with the chances of failure in the given area so as to provide suggestion and mitigation measures. In the field study the major landslide area of concern is taken as shown in the Figure 5. The results of Kinematic analysis of the study area using DIPS software are given in Figure 5.

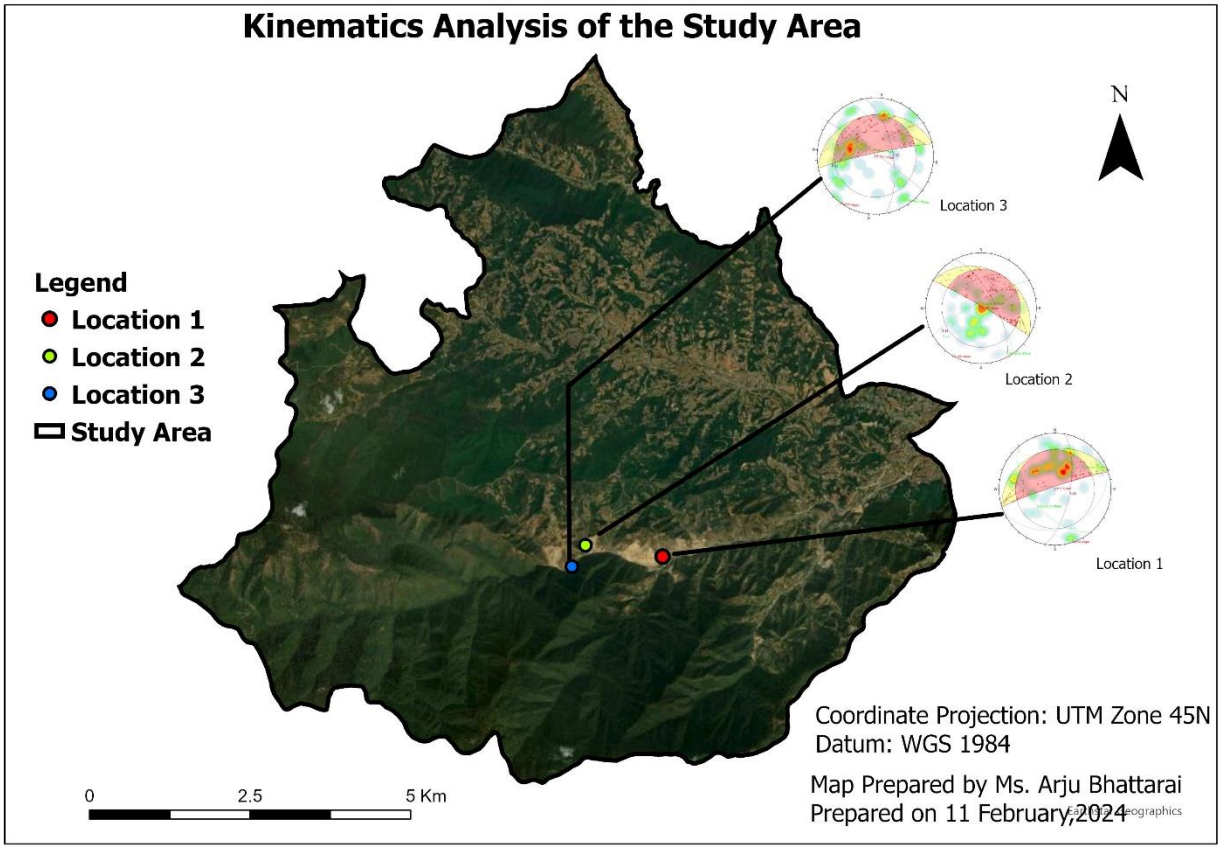

Figure 5: The map representing the point location of the data collection for kinematic analysis

Kinematic analysis aims to identify critical failure surfaces within the landslide mass. These surfaces represent the pathways along which sliding or failure is most likely to occur and are important for predicting potential landslide hazards. Hence the kinematic analysis is formed in the field investigation. The result of kinematic analysis performed in the three locations to study possible failures in the study area.

The detail of the kinematic analysis is given in Table 8.

Table 8: Details of possible failure in Landslide prone area.

Location	Slope Dip	Slope Dip Direction	Friction Angle	Failure Type	Failure in %
1	86°	342	30°	Wedge Failure Planar Failure Planar Failure(All) Flexural Toppling Direct Toppling	12% 6% 12% 18% 14%
2	86°	342	30°	Wedge Failure Planar Failure Planar Failure(All) Flexural Toppling Direct Toppling	19.4% 2% 26% 8% 8%
3	87°	30	30°	Wedge Failure Planar Failure Planar Failure(All) Flexural Toppling Direct Toppling	23.7% 5.7% 44.2% 25% 7.6%

4.3 Landside inventory Map

The first, and perhaps most crucial, stage in doing a susceptibility analysis for landslides is creating an inventory map of potential landslides. Understanding the circumstances and potential risk areas for future landslides is necessary for forecasting and assessing mechanisms governing previous landslides. This can be done by looking at the area's historical landslide activity. The hydrologic, topographic, and geologic conditions linked to previous landslides help identify whether naturally occurring or man-made conditions are most likely to result in landslides in the future. Three processes were taken to construct the area's landslide inventory map: fieldwork, interpretation of Google Earth images, and topological map analysis. The landslides marked on the topographic map of the Department of Survey, 1995 were updated by study of the Google Earth image of 2012 and then were verified and

further updated during fieldwork in 2015. The demarcation of the landslides on the topographic map was carried out in the field. These three approaches were coupled to prepare a reliable landslide distribution map in form of a point in the landslide inventory map.

From the landslide inventory map, the location of landslide is traced that maximum landslide is near to the built up areas the reason may be road construction, mining etc. From the landslide location data sets, the training and testing data are separated for the validation process the landslide inventory map representing Training and Testing data is shown in Figure 6

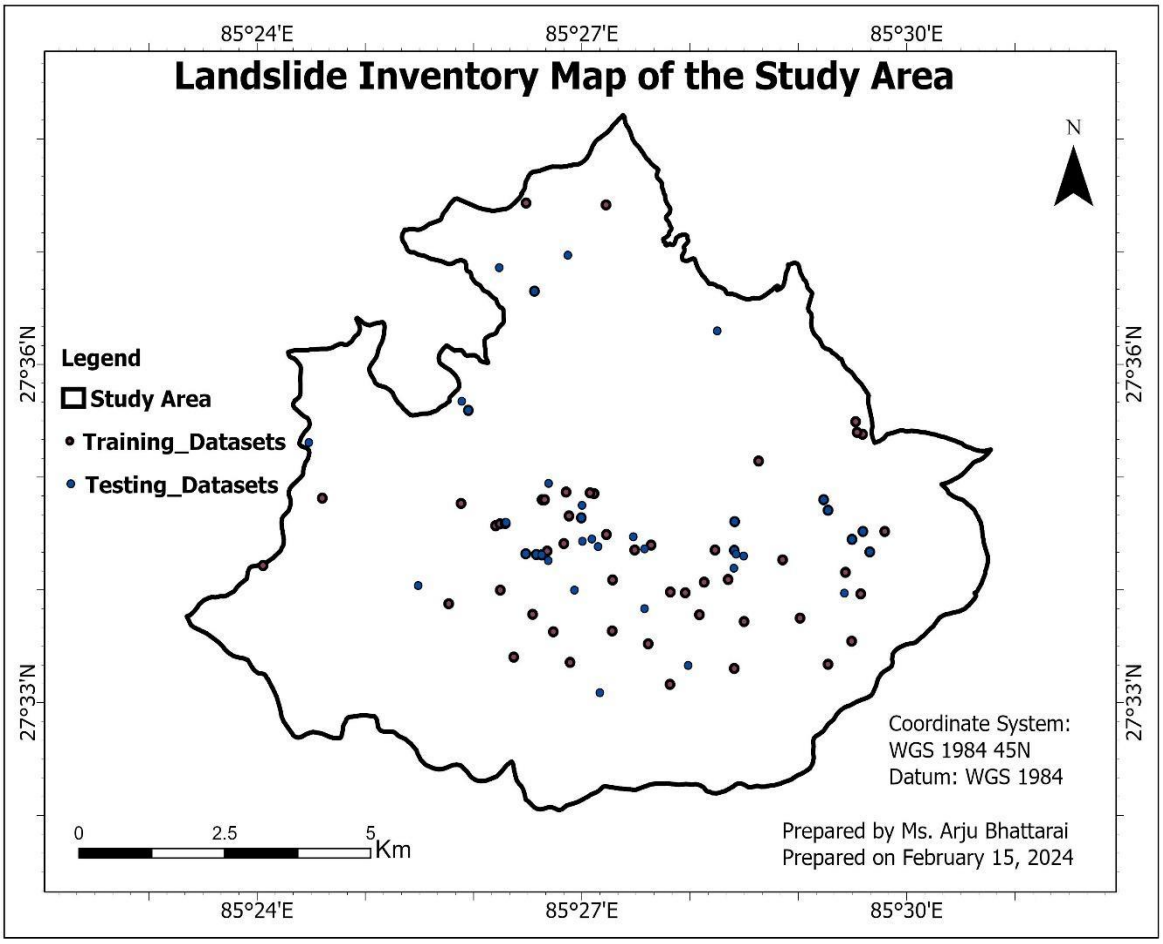

Figure 6: Map indicating testiong and training dataset of the study area.

Similarly, the polygon datasets of landslide in Figure 7 gives the total area of the study area covered by landslide. From the field investigation and Landslide inventory map from Google Earth. The inventory, the area of the landslide was found to be ranged from 9.2 to 44446.34 m^2. More landslide was found in built up areas and near road area however, various triggering factors have equal importance in inducing landslides.

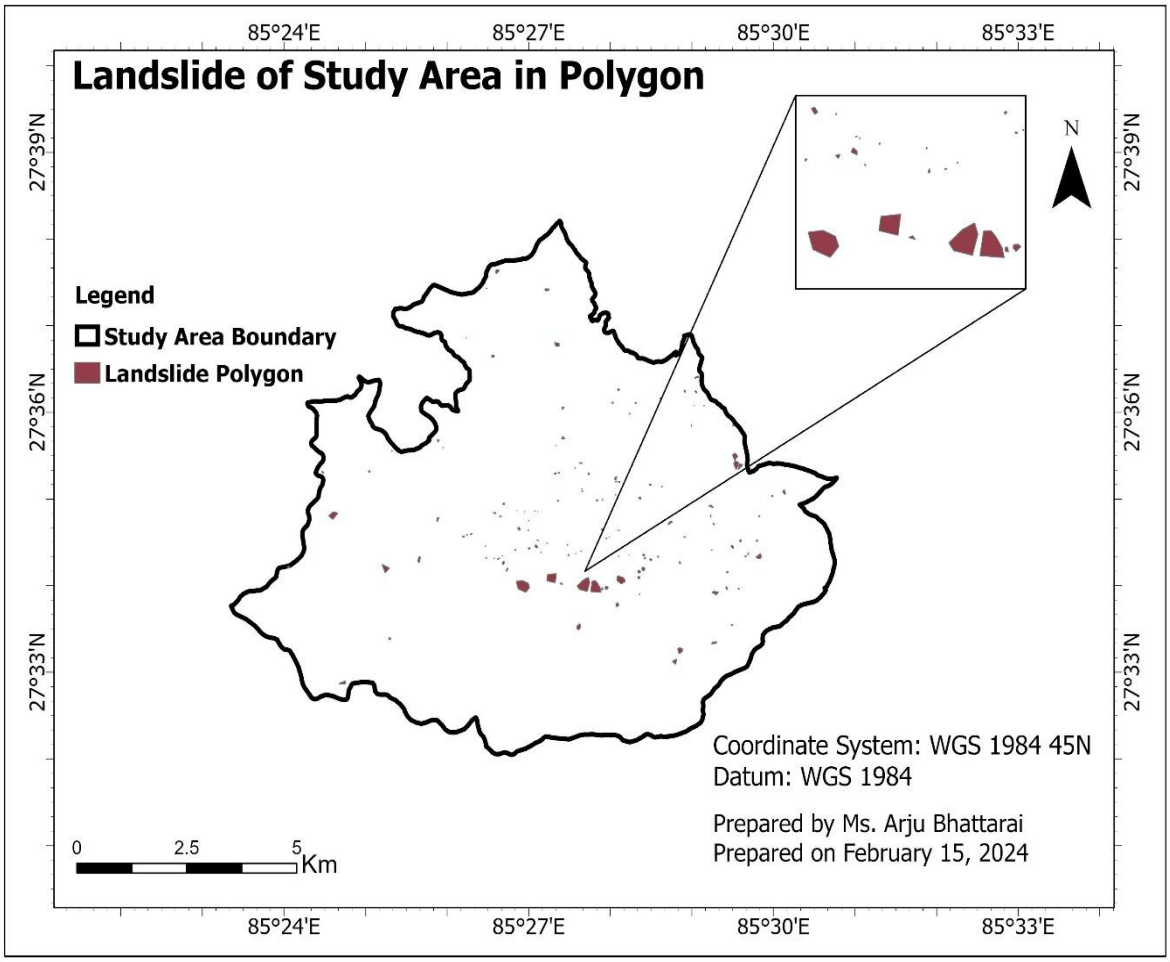

Figure 7: Map after digitizing landslide area in Polygon

4.4 Factors Affecting Landslide

4.4.1. Slope

Slope has a significant impact on surface and subsurface hydrology, as well as terrain stability. Landslide susceptibility estimates rely heavily on this characteristic. Moreover, literature review suggests steep slopes are very prone to landslide so, in this research the Slope map was prepared covering five classes: very low/flat (0°-15°), low (15°-30°), moderate (30°- 45°), high (45°- 60°) and very high (>60°) as shown in Figure 8.

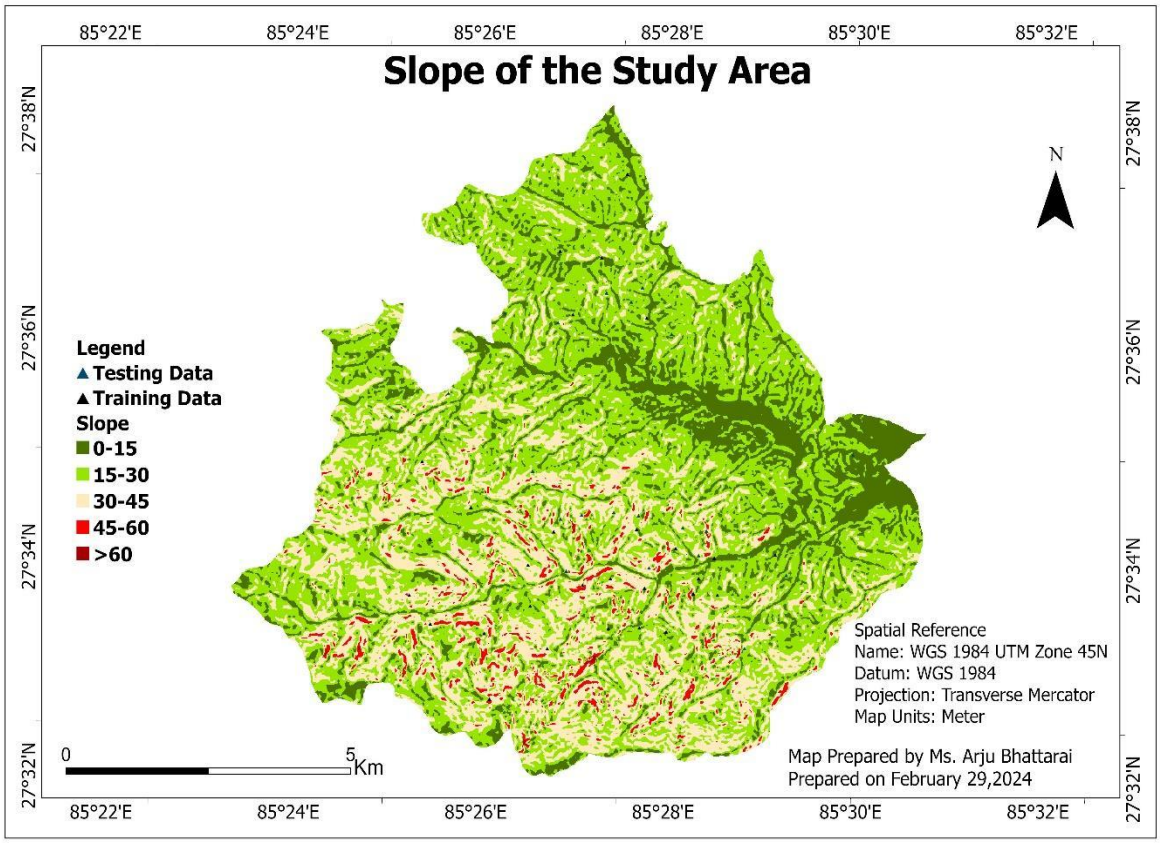

Figure 8: The Map representing slope of the study area.

The detail percentage and slide area in each slope classes are given in Table 9. Maximum landslides are seen in slope 30 degree to 40 degrees which is about 41.96 percentage minimum landslides area seen in slope greater than 60 degrees which is 0.33 percentage.

Table 9: Landslides in each classes of Slope

S.N.	Classes	Landslide Area(m2)	Landslide Pixel	Landslide%
1	0-15	37106.53	237	11.25
2	15-30	90965.81	581	27.58
3	30-45	137466.4	878	41.69
4	45-60	63096.76	473	19.13
5	60<	1095.974	7	0.33

4.4.2 Slope Aspect:

A slope's aspect refers to its orientation relative to the north. Literature review suggests slope aspect affects solar heating, soil moisture, and air dryness.

The slope aspect affects the stability of a terrain by regulating soil moisture and vegetation growth through sunshine exposure. For susceptibility analysis, aspect maps are divided into nine classes: N, NE, E, SE, S, SW, W, NW, and Flat. Landslides in different slope aspect is given in Table 8 the slope aspect of study area is shown in Figure 9.

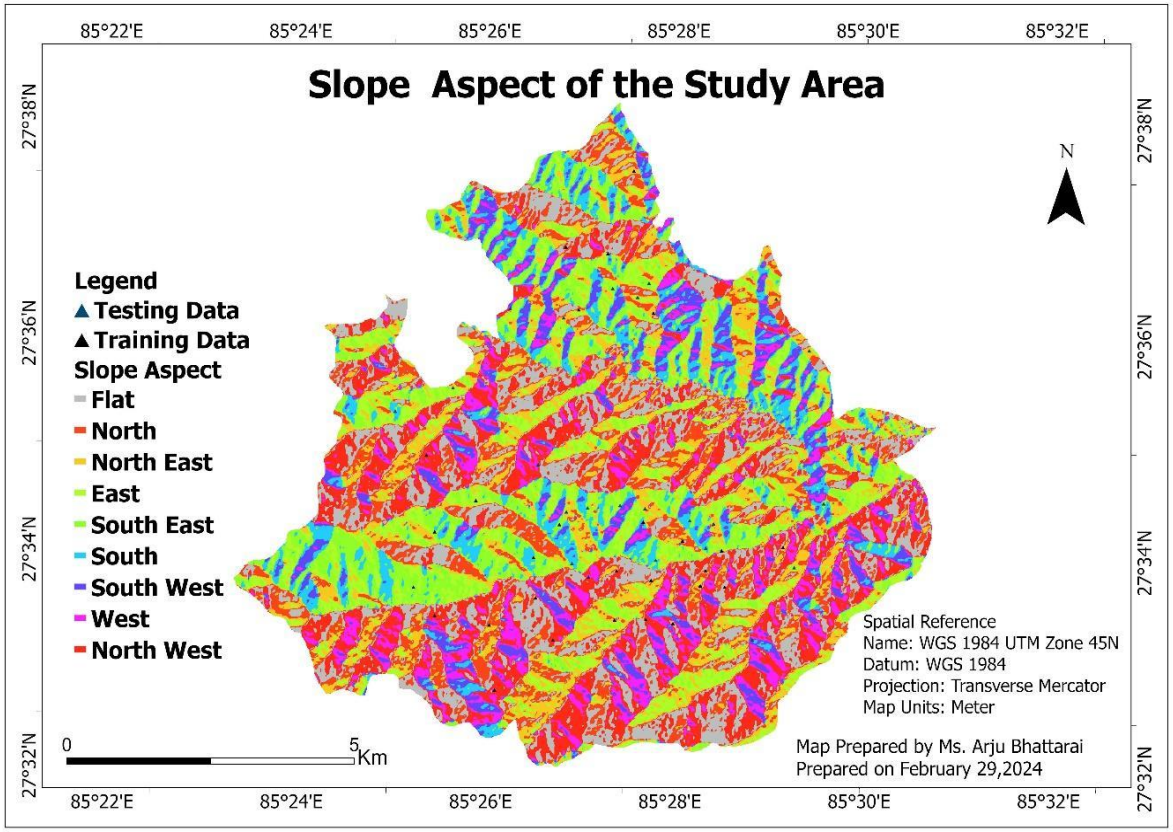

Figure 9: Slope Aspect Map of the study area.

In total landslides maximum of 30.63% of landslides are present in slope facing south whereas minimum 2.18% of landslide were found on slope facing west as given in Table 10.

Table 10: Landslide distribution with respect to each aspect classes

S. No.	Classes	Landslide Area (m^2)	Landslide Pixel	Landslide in %
1	Flat	12838.55	82	3.89
2	North	24424.55	156	7.41
3	North East	19884.09	127	6.03
4	East	38202.51	244	11.59
5	South East	95819.4	612	29.06
6	South	100986.1	645	30.63
7	South West	21136.63	135	6.41
8	West	7202.112	46	2.18
9	North West	9237.492	59	2.80

4.4.3 Lithology

Rocks of Kathmandu complex, Phulchauki Group were found in the study area. Mainly metasantstone, phyllite, slate were the dominant rocks present in the exposed area.

The lithology of study area consists of all the 6 formation i.e. Pulchauki Formation, Chitlang Formation, Tistung Formation, Chandragiri Formation and Sopyang Formation of Phulchauki group. The detail map showing the formation present in the study area is shown in the Figure 10.

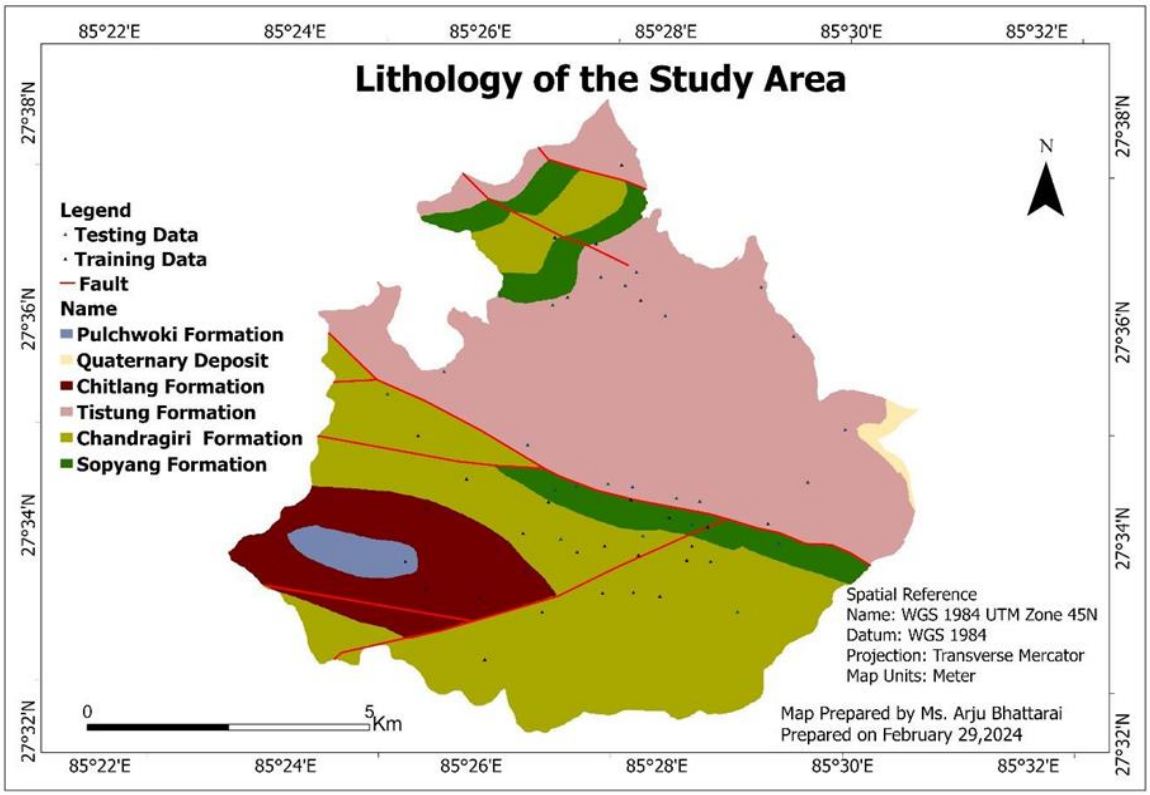

Figure 10: The map representing Lithology of Study area.

Maximum landslides were seen in Chandragiri formation covering area of 50312.5m2.

Note: No landslides were seen on Phulchauki Formation as shown in Table 11. Also, Godavari landslide is the youngest formation of entire Kathmandu Nappe.

Table 11. Landslide distribution with respect to each Formation.

S. No.	Classes	Landslide Pixel	Area (m^2)	Landslide in %
1	Tistung Formation	484	75625	22.88
2	Quaternary Deposit	2	312.5	0.094
3	Sopyang Formation	322	50312.5	15.22
4	Chandragiri Formation	1230	192187.5	58.15
5	Chitlang Formation	77	12031.25	3.64
6.	Phulchauki Formation	-	-	-

4.4.4 Road:

The road network can significantly influence the occurrence of landslides. Building roads on unstable terrain increases the risk of landslides. Figure 11 shows the distribution of landslide events at various distances from the road network. Also in the map it is divided into three classes 0-1300m, 1300-2600m and 2600-4000m.

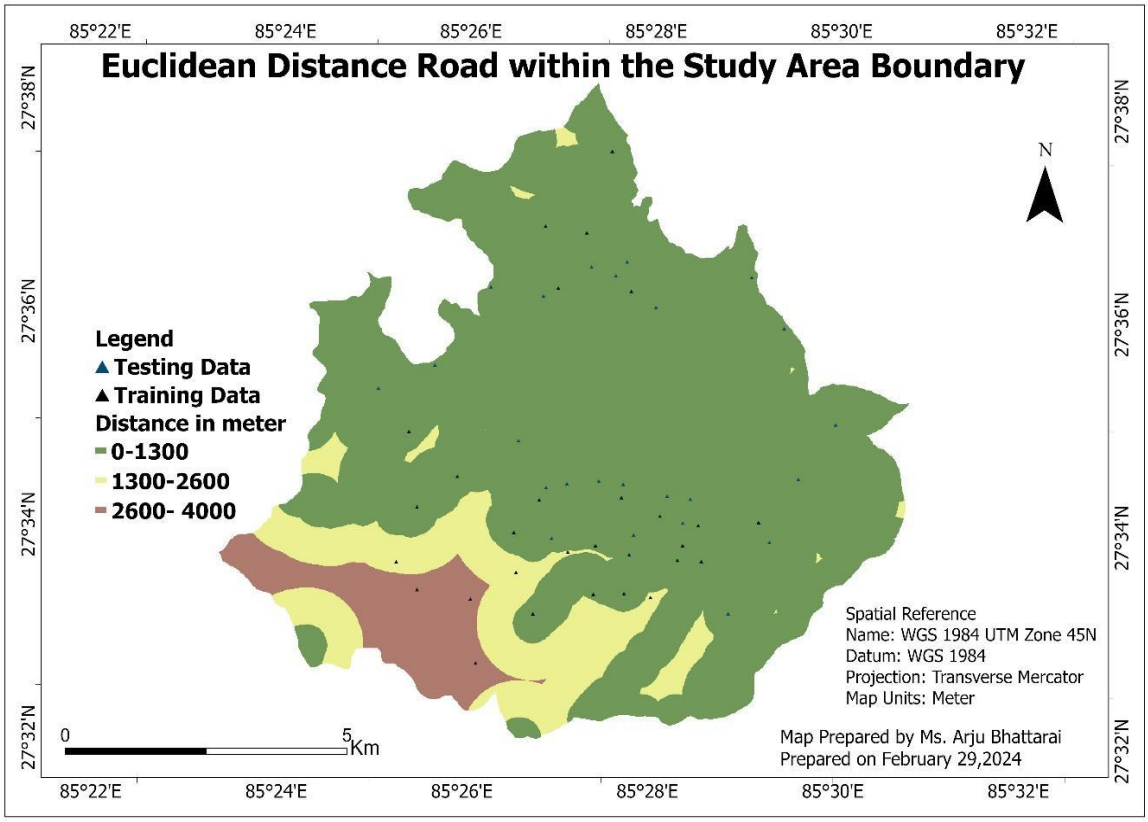

Figure 11: The map representing Euclidean Distance of Road with the study area Boundary.

Additional in Table 12 maximum landslide is seen near to the road distance i.e. 98 percentage of landslide is very close 0-1300m distance to the road network.

Table 12: Landslide distribution in each classes of Euclidean Road distance

S. No.	Classes	Landslide Pixel	Landslide Area (m^2)	Landslide in %
1	0-1300	2084	325625	98.72099
2	1300-2600	24	3750	1.136902
3	2600-4000	7	1093.75	0.331596

4.4.5 Fault:

Fault distance is crucial in landslide occurrences as it directly influences the potential for slope instability. The proximity of a fault to a slope can amplify the risk of landslides due to the geological and tectonic forces associated with fault activity. Closer fault distances often result in increased stress and strain on the slope, heightening the likelihood of slope failure and triggering landslides. As shown in the Figure 12 Euclidean distance of existing fault is classified into three classes' i.e. 0-1300, 1300-2600 and greater than 2600 in meters and the presence of landslide in each classes is given in Table 13.

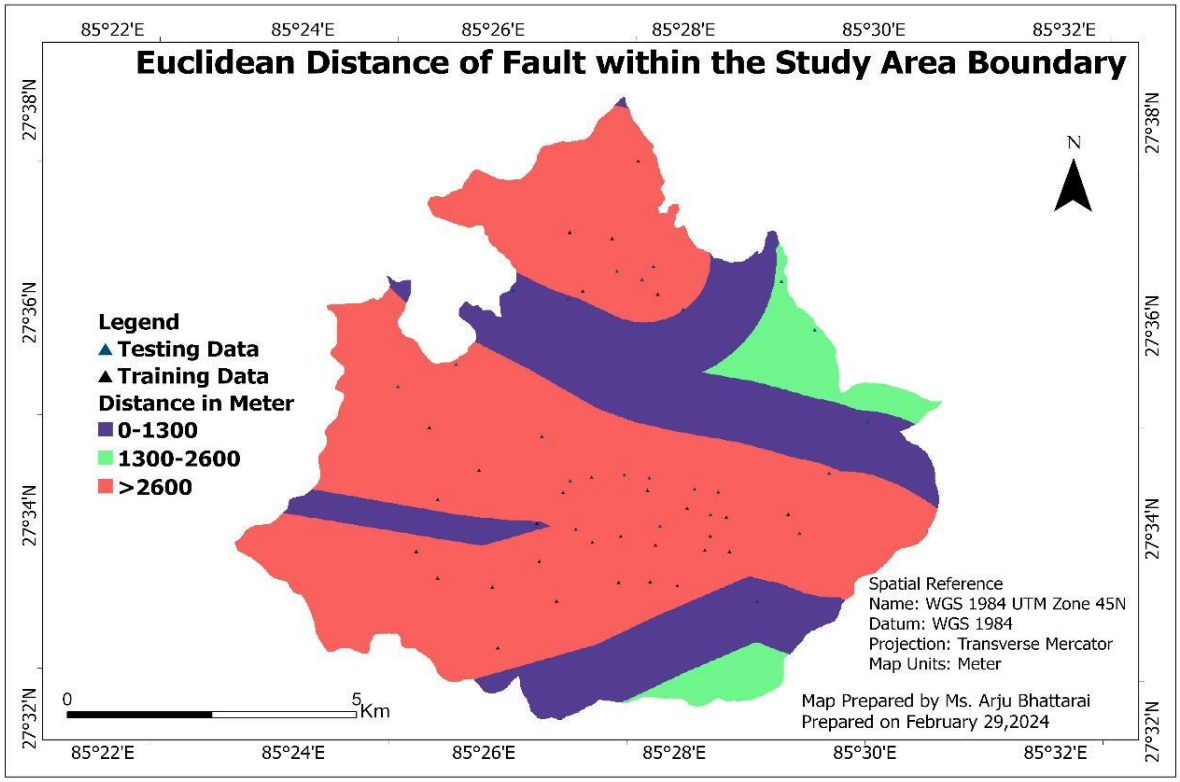

Figure 12: The Map representing Euclidean Distance of Fault within the Boundary of Study area.

The presence of landslide in each classes is given in Table 13.Here maximum landslide of 82.93% is seen in between the 0-1300m distance classes of total landslide area of 274062.5m^2

Table 13: Landslide distribution in each classes of Euclidean Fault distance

S. No.	Classes	Landslide Pixel	Landslide Area (m^2)	Landslide in %
1	0-1300	1754	274062.5	82.93144
2	1300-2300	201	31406.25	9.503546
3	2300<	160	25000	7.565012

4.4.6 Drainage:

Landslides were frequently observed along the research area's stream. The location of the landslide from the stream was deemed a geomorphology-related causal element. Field observations show that slope failure occurs more frequently along streams due to groundwater migration and toe undercutting. A distance to drainage map was created for landslide activity analysis and susceptibility evaluation as shown in Figure13.

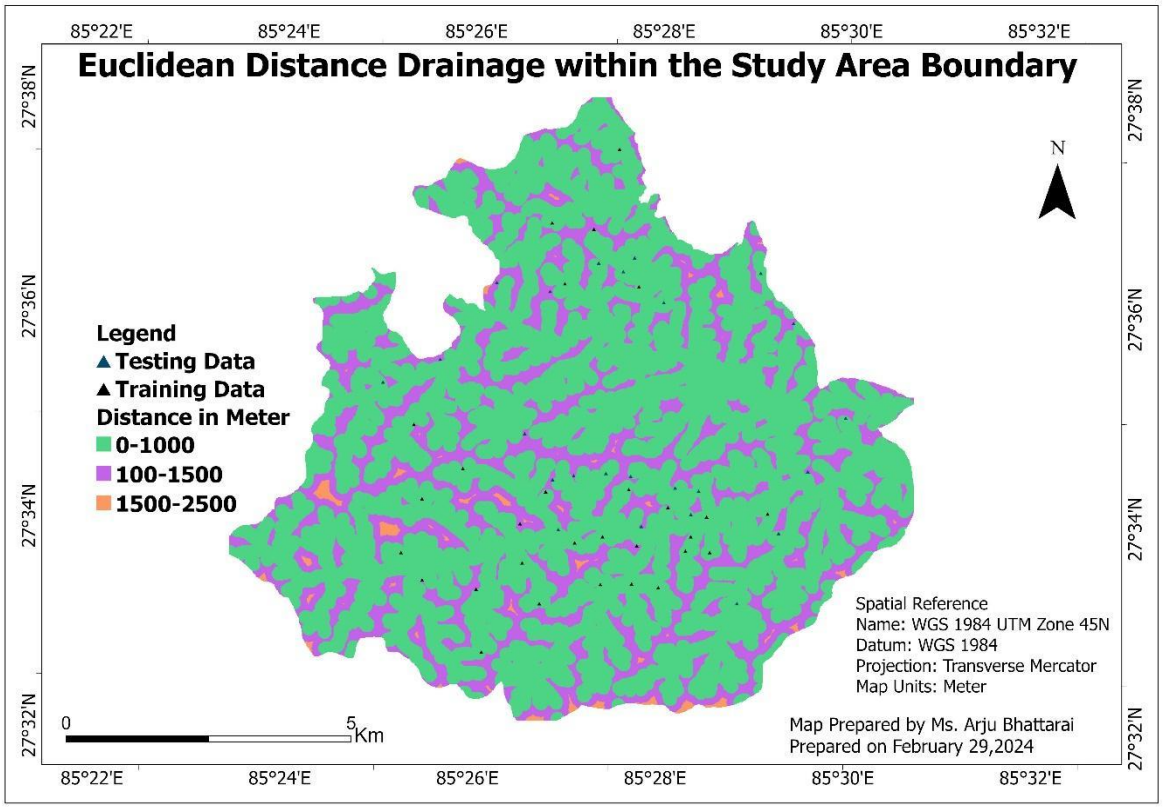

Figure 13: The Map representing Euclidean Distance of Drainage within the Boundary of Study area

In the below Table 14 maximum landslides are seen on a distance near to drainage maximum landslide pixel of 1636 is found. Least landslides are found in distance farther then drainage.

Table 14: Landslide distribution in each classes of Euclidean Drainage Distance

S. No.	Classes	Landslide Pixel	Landslide Area (m^2)	Landslide in %
1	0-1000	1636	255625	77.35225
2	1000-1500	478	74687.5	22.60047
3	1500-2500	1	156.25	0.047281

4.4.7 Land Use Land Cover

Land cover always controls the landslide process. Well-forested slopes are less prone to landslides. Land cover always controls the landslide process. Slopes in forest areas are always lower. prone to landslide occurrence whereas unmanaged built up areas and cultivation also drainage like water stream could induce landslide. In the Figure 14 LULC map of the study area it is divided into five classes i.e. Water, developed, Barren, Forest, Planted/ cultivated Figure 14.

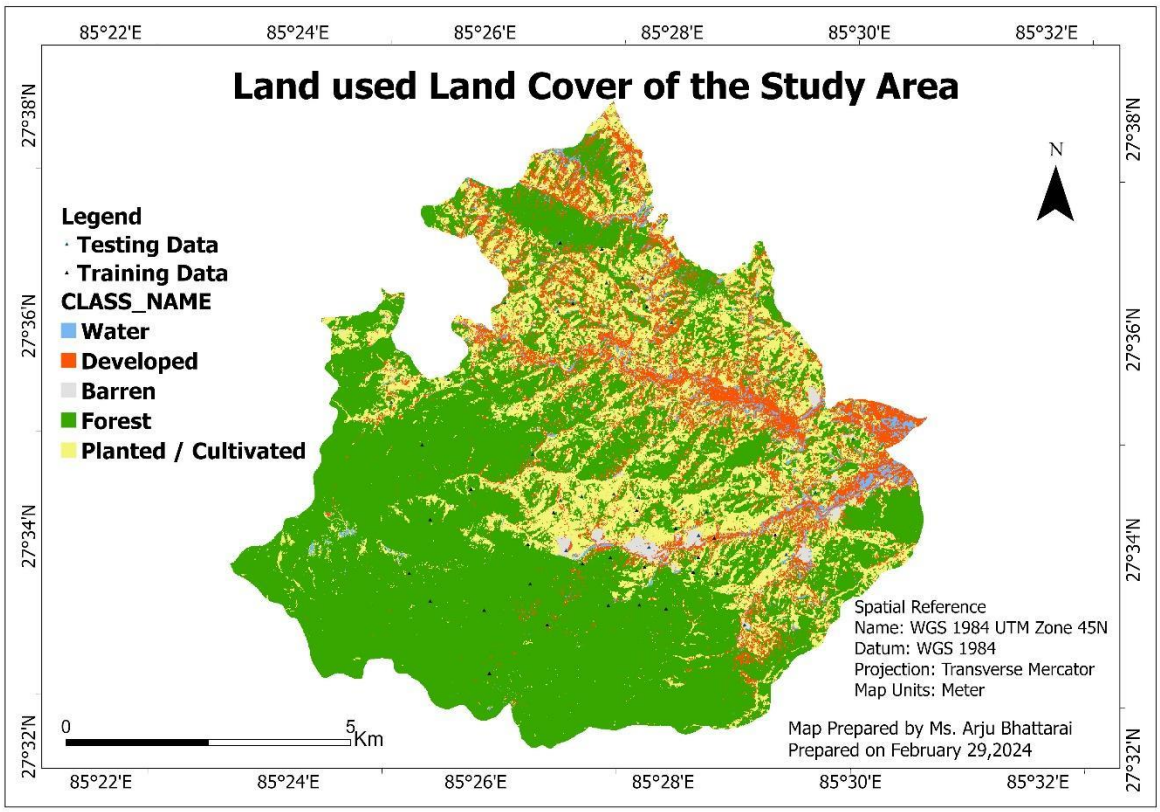

Figure 14: The map representing the Land Use Land Cover Map of the study area.

Additionally, as given in Table 15 maximum landslide percentage is seen in barren land followed by planted and cultivated areas. However, the least landslides 0.94% is seen in water areas.

Table 15: Landslide distribution in each classes of Land Use Land Cover

S. No.	Classes	Landslide Pixel	Landslide Area (m^2)	Landslid %
1	Water	20	31250	0.945626
2	Developed	213	242812.5	10.07092
3	Barren	1208	45000	57.11584

4	Forest	145	5625	6.855792
5	Planted / Cultivated	529	5781.25	25.01182

Accuracy Assessment of LULC Map:

This method often involves comparing the classified map to reference data, which can be obtained by field surveys or high-resolution imaging. Accuracy evaluation criteria, such as overall accuracy, producer accuracy, user accuracy, and the Kappa coefficient, are frequently employed to quantify the dependability of the LULC categorization. These criteria aid in determining the agreement between the mapped classes and the genuine land cover, providing useful information for increasing the accuracy of land cover mapping methodologies. The Kappa coefficient of LULC map is 0.865 which means 85% accurate and P_Accuracy 93% as given in Table 16.

Table 16: Accuracy Assessment of Land Use Land Cover Map

I.D	Class Value	C_1	C_2	C_3	C_4	C_5	Total	U_Accuracy	Kappa
1	Water	1	0	0	0	0	1	1	0
2	Developed	0	7	0	2	1	10	0.7	0
3	Barren	0	0	2	0	1	3	0.67	0
4	Forest	0	0	0	62	1	63	0.98	0
5	Planted/ Cultivated	0	0	0	2	21	23	0.91	0
6	Total	1	7	2	66	24	100	0	0
7	P_Accuracy	1	1	1	0.93	0.87	0	0.93	0
8	Kappa	0	0	0	0	0	0	0	0.86

4.4.8 Rainfall:

Rainfall is extrinsic parameter it had been used with susceptibility map for producing landslide in the study area. For the average annual rain fall data preparation 13 years' data in the format of CSV file was used of 6 rainfall station as shown in Figure 15 and it was categorized into 5 classes i.e.1028-1038, 1038-1048, 1048-1058, 1058-1068, 1068-1080 in mm.

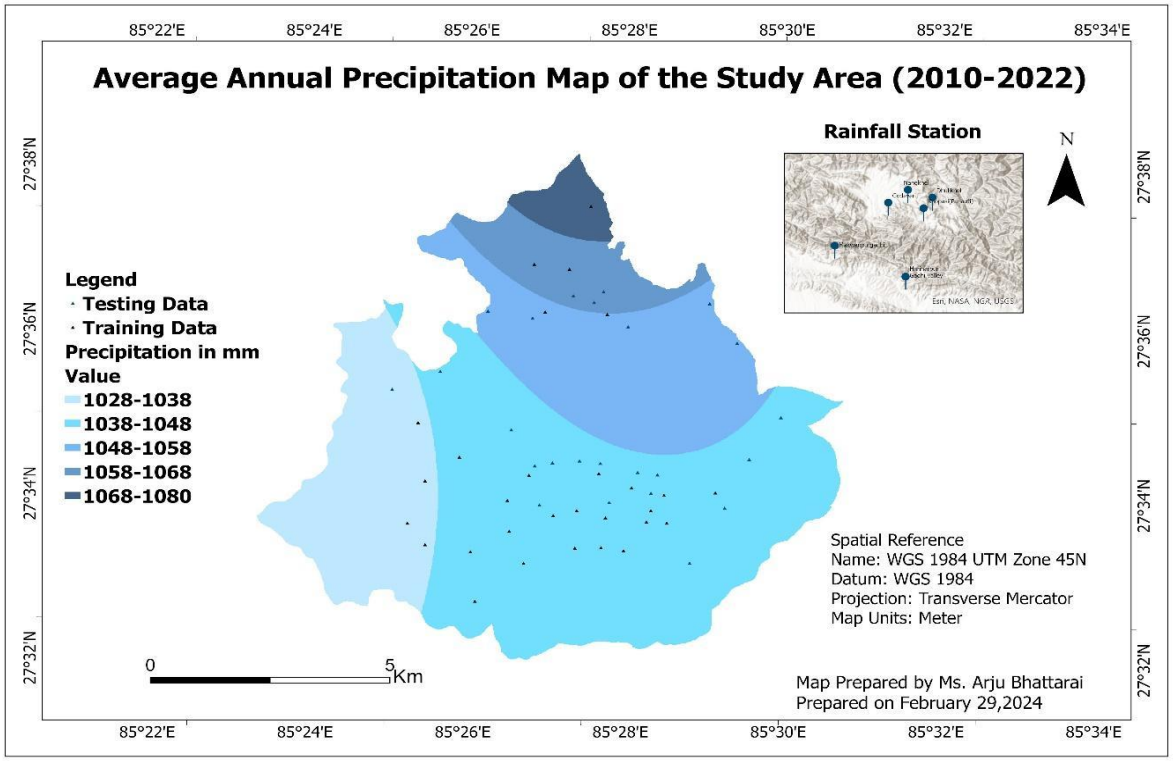

Figure 15: Average Annual precipitation map of the study area (2010-2012)

In the below illustrated Table 17 Maximum landslide is seen in classes 1038-1048 and minimum landslide of 1.07% is seen in classes 1078-1080.

Table 17: Landslide in 5 different classes of Precipitation.

S. No.	Classes	Landslide Pixel	Landslide Area (m^2)	Landslide in %
1	1028-1038	200	31250	9.456265
2	1038-1048	1554	242812.5	73.47518
3	1048-1058	288	45000	13.61702
4	1058-1068	36	5625	1.702128
5	1078-1080	37	5781.25	1.749409

4.4.9 Topographic Wetness Index (TWI)

TWI from DEM is a widely used method for assessing soil moisture, with altering TWI values influencing both moisture and species (Kopecký et al., 2021). The distribution of landslides across various TWI classes is clearly apparent in the Figure 16 and it is classified in 4

categories i.e. 0-7, 7-12, 12-17, 17-23. Maximum landslide is seen in range 0-7 where the landslide area is 292500m2.

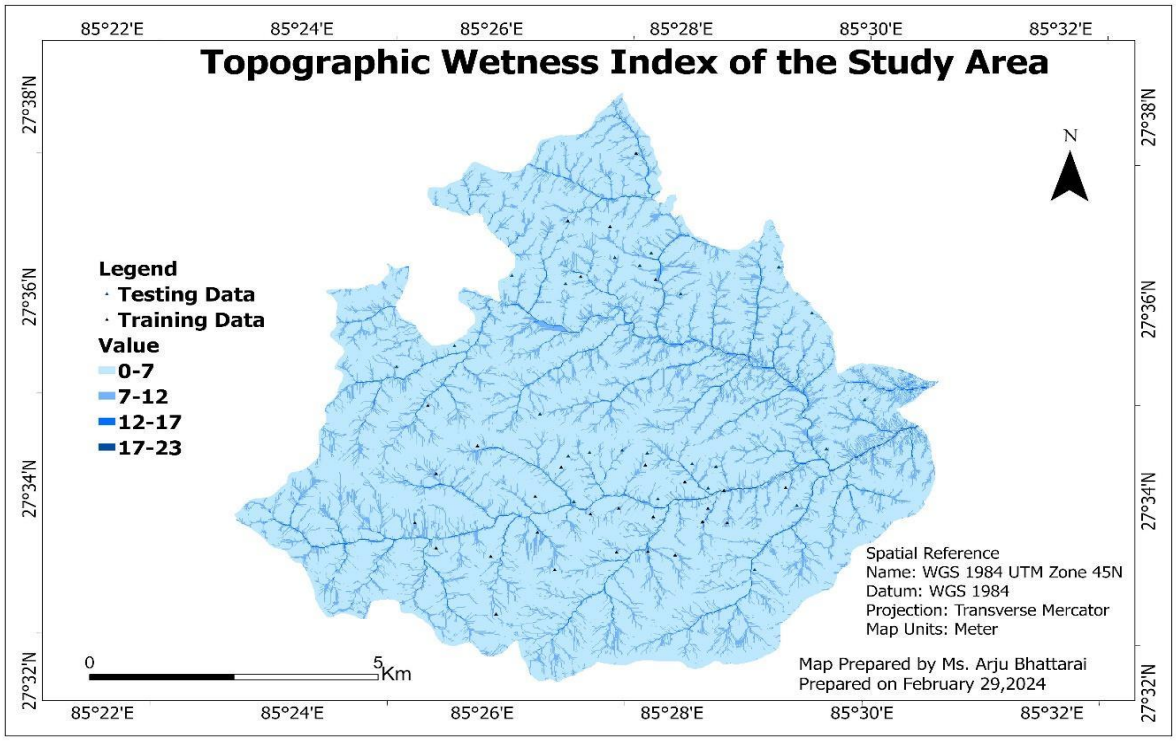

Figure 16: Map representing Topographic Wetness Index of study area

In Table 18 Maximum landslide is seen in range 0-7 where the landslide area is 292500m2 and minimum landslide of area 156.25 m2 is seen in range 17-23.

Table 18: Landslide in different classes of Topographic Wetness Index

S. No.	Classes	Landslide Pixel	Landslide Area (m^2)	Landslide in %
1	0-7	1872	292500	88.51064
2	7.0-12	217	33906.25	14.57354
3	12-17.0	25	3906.25	3.99361
4	17-23	1	156.25	0.047281

4.4.10 Slope curvature:

Curvatures, along with other parameters, influence water flow in and out of slopes, making them crucial for studying landslides this study focused on profile curvature. A profile curvature map was created, depicting both concave and convex profiles as shown in the Figure 17. Similarly, the table shows the landslide coverage in each classes.

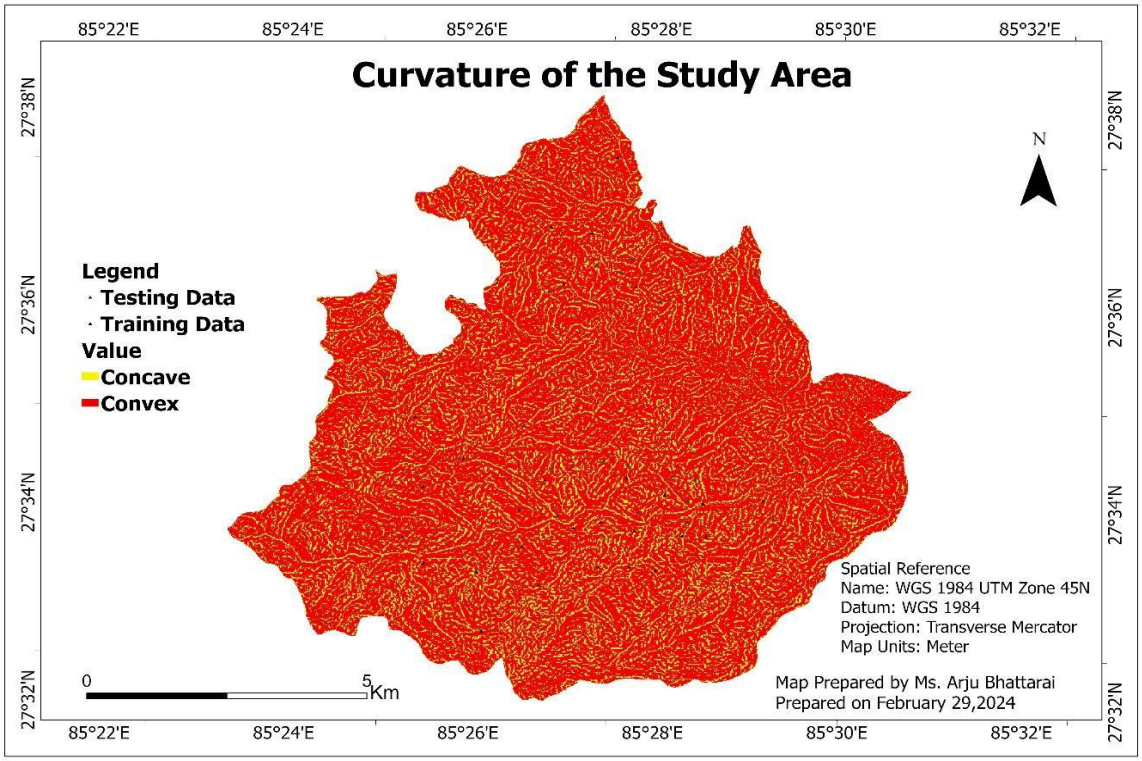

Figure 17: Map showing the curvature of the study area.

Maximum Landslide is seen in the concave curvature i.e. about 77 percentages as in Table 19.

Table 19: Landslide Present in each classes of slope curvature

S. No.	Classes	Landslide Pixel	Landslide Area (m^2)	Landslide in %
1	Concave	1489	232656.3	77
2	Convex	626	97812.5	22.9

4.4 Landslide Susceptibility Mapping

In this study, Landslide Susceptibility Index Map was created by using FR and AHP methods.

4.5.1 Analytical Hierarchy Process Method

Table 20: The pair-wise comparison matrix, class weights (rating) and consistency ratio

Matrix		1	2	3	4	5	6	7	8	9	10	weightage
Slope	1	1	1	1	2	1	1	1	1	1/2	1	9.58%
Aspect	2	1	1	1	2	1	4	1	1	2	2	13.19%
Lithology	3	1	1	1	4	3	1	1	1	2	4	15.40%
LULC	4	1/2	1/2	1/4	1	2	2	1/2	1	2	4	9.92%
Distance to Fault	5	1	1	1/3	1/2	1	1	2	1	1	4	9.67%
Distance to Drainage	6	1	1/4	1	1/2	1	1	1	1/3	1	2	7.39%
Distance to Road Network	7	1	1	1	2	1/2	1	1	1	1	4	10.56%
Precipitation	8	1	1	1	1	1	3	1	1	1	4	11.44%
TWI	9	2	1/2	1/2	1/2	1	1	1	1	1	4	9.21%
Curvature	10	1	1/2	1/4	1/4	1/4	1/2	1/4	1/4	1/4	1	3.65%

CR= 6.2%

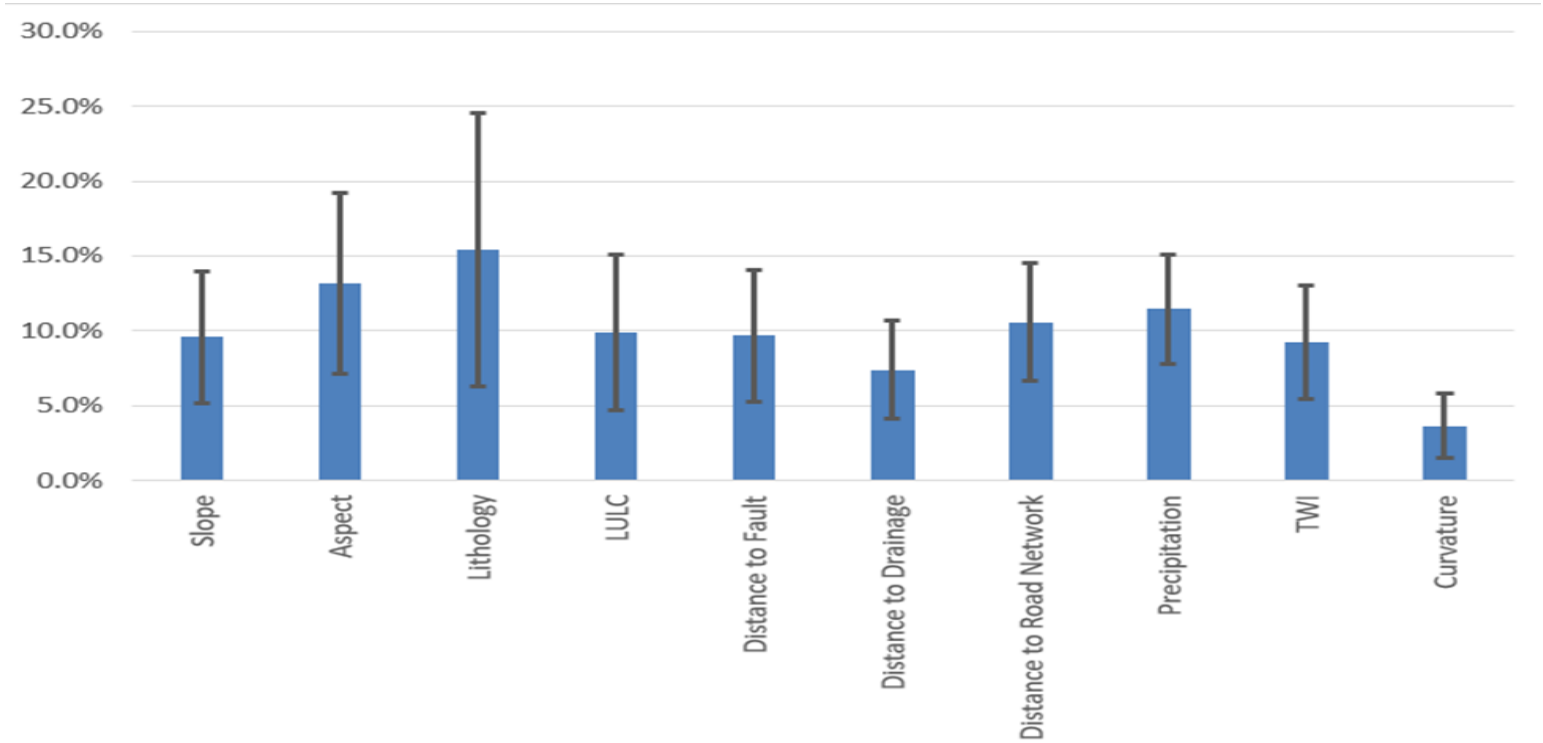

Figure 18: Bar graph representing the factors in corresponding to their weightage

The bar graph Figure 18 represents the percentage weightage given to factors.

Comparison matrix of all the 10 factors with each classes

Table 21: The pair-wise comparison matrix, class weights (rating) and consistency ratio

Slope Matrix		0-15	15-30	30-45	45-60	60<	**Weightage**
		1	2	3	4	5	
0-15	1	1	1	1/5	1/5	1/5	**8.85%**
15-30	2	1	1	1	5	5	**36.60%**
30-45	3	5	1	1	1	1	**21.25%**
45-60	4	5	1/5	1	1	1	**16.65%**
60<	5	5	1/5	1	1	1	**16.65%**

CR= 7%

Aspect Matrix		Flat	North	North East	East	South East	South	South West	**Weightage**
		1	2	3	4	5	6	7	
Flat	1	1	1 2/5	5/8	5/8	1/5	4/9	4/9	**7.57%**
North	2	5/7	1	1	2 1/4	1	4/9	4/9	**9.96%**
North East	3	1 4/7	1	1	1	4/7	4/9	4/7	**9.16%**
East	4	1 4/7	4/9	1	1	1	1	1	**10.44%**
South East	5	5	1	1 3/4	1	1	1	1	**15.06%**
South	6	2 1/4	2 1/4	2 1/4	1	1	1	1	**15.04%**
South West	7	2 1/4	2 1/4	1 3/4	1	1	1	1	**14.56%**
West	8	5/7	1	5/7	1	4/7	4/9	4/9	**7.64%**

CR= 6.8%

Lithology Matrix		Quaternary Formation	Chandragiri Formation	Sopyang Formation	Tistung Formation	Chitlang Formation	**Weightage**
		1	2	3	4	5	
Quaternary Formation	1	1	1	5/8	4/7	5/7	**15.07%**
Chandragiri Formation	2	1	1	1 3/4	2	1 2/9	**26.53%**
Sopyang Formation	3	1 4/7	4/7	1	1 2/5	4/5	**19.60%**
Tistung Formation	4	1 3/4	1/2	5/7	1	1 3/4	**20.20%**
Chitlang Formation	5	1 2/5	4/5	1 2/9	4/7	1	**18.60%**

CR=6%

Road Matrix		0-1300	1300-2600	2600-4000	**Weightage**
		1	2	3	
0-1300	1	1	2 1/4	3 1/6	**56.88 %**
1300-2600	2	4/9	1	1 2/9	**24.25 %**
2600-4000	3	1/3	4/5	1	**18.87 %**

CR= 4%

Fault Matrix		0-1300	1300-2300	2300<	**Weightage**
		1	2	3	
0-1300	1	1	2 1/4	3 1/6	**56.88%**
1300-2300	2	4/9	1	1 2/9	**24.25%**
2300<	3	1/3	4/5	1	**18.87%**

CR=4%

Drainage Matrix		0-1000	1000-1500	1500-2500	Weightage
		1	2	3	
0-1000	1	1	2 1/4	3 1/6	**54.88%**
1000-1500	2	4/9	1	1 2/9	**25.25%**
1500-2500	3	1/3	4/5	1	**18.87%**

CR=4%

Precipitation Matrix		1028-1038	1038-1048	1048-1058	1058-1068	1078-1080	Weightage
		1	2	3	4	5	
1028-1038	1	1	1	1 2/5	1 2/5	1 2/5	**23.55%**
1038-1048	2	1	1	1 3/4	2 4/9	5/7	**24.67%**
1048-1058	3	5/7	4/7	1	1 3/4	1	**17.99%**
1058-1068	4	5/7	2/5	4/7	1	1	**13.75%**
1078-1080	5	5/7	1 2/5	1	1	1	**20.04%**

CR=3.5%

LULC Matrix		Water	Developed	Barren	Forest	Planted / Cultivated	Weightage
		1	2	3	4	5	
Water	1	1	1	1 2/5	1 2/5	1 3/4	**24.78%**
Developed	2	1	1	1 3/4	2 4/9	5/7	**24.46%**
Barren	3	5/7	4/7	1	1	4/7	**14.23%**
Forest	4	5/7	2/5	1	1	1	**15.18%**
Planted / Cultivated	5	4/7	1 2/5	1 3/4	1	1	**21.35%**

CR=5%

TWI Matrix		0-7	7.0-12	12-17.0	17-23	Weightage
		1	2	3	4	
0-7	1	1	1	1 2/5	1 2/5	**28.60%**
7.0-12	2	1	1	1 3/4	2 4/9	**34.64%**
12-17.0	3	5/7	4/7	1	1	**19.11%**
17-23	4	5/7	2/5	1	1	**17.65%**

CR=2%

Curvature Matrix		Concave	Convex	Weightage
		1	2	
Concave	1	1	2 1/4	**69.10%**
Convex	2	4/9	1	**30.90%**

CR=1.1%

In the above Table 20 maximum weightage is given to lithology which is about 15% because the weathering properties of rocks and soils impact their stability. Certain lithological formations may undergo chemical or physical weathering more rapidly, leading to increased susceptibility to landslides. In the case of the study area Chandragiri Formation is highly susceptible to landslide with a maximum weightage of about 26.53% as shown in Table 21. In the study area, minimum weightage is given to curvature i.e. 3.65%. When observing each class of curvature concave has maximum weightage as shown in Table 20. The slope is also a very important causative factor the slope ranges 30-45 has given a maximum weightage of 36 percent and in Table 21. In Table 20, 9.58 percentage weightage is given to slope in comparison matrix with respect to the other 9 causative factors. When researching about the

aspect southern part of the slope is always prone to landslides hence maximum weightage is given to the southern part of the aspect and the aspect is given 13.19%. In comparison to landslides in forest areas, barren areas are more prone to landslides. For the lithology of overall study area total weightage of 9.92%. Overall for the Road, Fault, and Drainage nearer the distance the greater is weightage given because the chance of occurring landslide is more near to road cuts, rivers and faults. Their respective weightage given are 10, 7, and 9 when converting it into an integer. The extrusive factor of landslide among 10 causative factors is rainfall. The weightage given to precipitation according to Table 20 is 11.4%. For the TWI index, the weightage of 9.21 % is given.

4.5.2 Landslide Susceptibility Map from AHP Method:

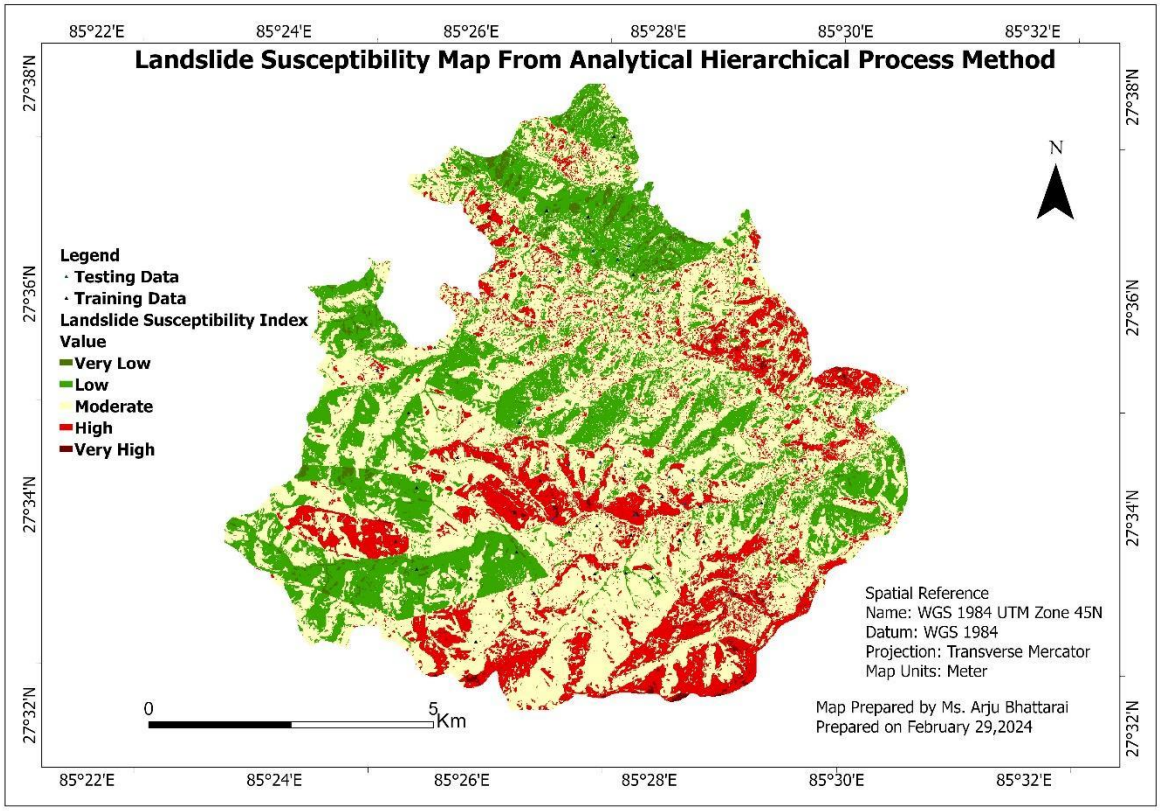

Figure 19: Landslide Susceptible map From AHP Method

LSM was accomplished using the AHP approach as shown in Figure 19. AHP was used to weight factors and classes. Raster maps of each factor were weighted on a cell-by-cell basis. The integration of weighted raster map produced an LSM map containing numerical

susceptibility data, with higher LSI values indicating high susceptibility and lower values indicating low susceptibility. LSI values vary from 6.58 to 37.

Now the distribution of landslide susceptibility zones and landslide occurrence is given in Table 22

Table 22: The distribution of landslide susceptibility zones and landslide occurrence

Susceptibility Classes	Class Pixel	Percentage	Landslide Pixel	Landslide%	Landslide Area
Very Low	7532	1.53	9	0.42	937
Low	137632	27.89	144	6.8	2261.65
Moderate	258261	52.34	530	25.05	82812.5
High	87568	17.75	1253	59.243	195781.3
Very High	2408	0.49	179	8.463	27968.75
Sum	493401		2115		

In the Table 22 maximum class percentage of 52.34 is in moderate zone, 0.49 which least percentage is observed in very high zone.

4.5.3 Frequecy Ratio Method:

Table 23 : Frequency ratio of 10 causative factors

Parameters	Classes	Class Pixel	%Class Pixels	Landslide Pixels	%Landslide Pixel)	FR	RF	RF(non%)	RF(Int)	Min RF	Max RF	Max-Min RF	(Max-Min)Min RF	PR
Slope	0-15	66924	13.54	237	11.25	0.003	0.16	16.31	16					
	15-30	185710	37.59	581	27.58	0.003	0.14	14.41	14					
	30-45	189009	38.26	878	41.69	0.004	0.214	21.40	21					
	45-60	49074	9.93	403	19.13	0.008	0.378	37.83	37					
	60<	3213	0.65	7	0.33	0.002	0.100	10.03	10					
Sum		493930	100	2106	100	0.021				0.10	0.37	0.27	0.14	1.94
Aspect	Flat	80292	16.25	82	3.89	0.0010	0.022	2.23	2					
	North	58094	11.75	156	7.42	0.0026	0.058	5.86	5					
	North East	58429	11.82	127	6.03	0.0021	0.047	4.750	4					
	East	62783	12.70	244	11.58	0.0038	0.084	8.494	8					
	South East	49291	9.97	612	29.05	0.0124	0.271	27.13	27					
	South	36695	7.42	645	30.62	0.0175	0.384	38.42	38					
	South West	33404	6.76	135	6.41	0.004	0.088	8.833	8					
	West	39337	7.96	46	2.18	0.001	0.025	2.556	2					
	North West	75743	15.33	59	2.80	0.0007	0.017	1.70	1					
Sum		494068	100	2106	100	0.045				0.017	0.384	0.367	0.143	2.56
Lithology	Tistung Formation	211138	43.20	484	22.88	0.002	0.116	11.67	11					
	Quaternary Deposit	3198	0.65	2	0.09	0.0006	0.03	3.18	3					
	Sopyang Formation	37561	7.68	322	15.22	0.0085	0.436	43.65	43					
	Chandragiri Formation	183348	37.51	1230	58.15	0.0067	0.341	34.15	34					
	Chitlang Formation	53457	10.93	77	3.64	0.0014	0.073	7.33	7					
Sum		488702	100	2115	100	0.0196				0.031	0.436	0.404	0.143	2.82
Distance From Road	0-1300	435124	87.43	2084	98.72	0.0047	0.832	83.239	83					
	1300-2600	47170	9.47	24	1.13	0.0005	0.088	8.842	8					
	2600-4000	15367	3.08	7	0.33	0.0004	0.079	7.9168	7					
Sum		497661	100	2115	100.1895	0.0057				0.0791	0.832	0.75	0.143	5.25
Distance From Fault	0-1300	326691	72.57	1754	82.93	0.005	0.453	45.300	45					
	1300-2300	139216	30.92	201	9.50	0.001	0.121	12.181	12					
	2300<	20407	4.53	160	7.56	0.005	0.425	42.51	42					
Sum		486314	108.03	2115	100	0.0118				0.121	0.453	0.331	0.143	2.31
Distance From Drainage	0-1000	371704	74.81	1636	77.35	0.0044	0.512	51.208	51					
	1000-1500	121037	24.36	478	22.60	0.003	0.459	45.947	45					
	1500-2500	4086	0.82	1	0.047	0.0002	0.028	2.847	2					
Sum		496827	100	2115	100	0.0085				0.028	0.512	0.483	0.143	3.37
Precipitation	1028-1038	90278	18.14	200	9.456	0.002	0.151	15.101	15					
	1038-1048	251557	50.54	1554	73.47	0.006	0.421	42.109	42					
	1048-1058	105030	21.10	288	13.61	0.002	0.1869	18.691	18					
	1058-1068	36241	7.28	36	1.702	0.0009	0.067	6.771	6					

	1078-1080	14555	2.92	37	1.749	0.0025	0.1732	17.32	17					
Sum		497661	100	2115	100	0.01467				0.067	0.421	0.353	0.143	2.46
LULC	Water	19359	2.48	20	0.94	0.001	0.0064	0.64	0					
	Developed	95337	12.26	213	10.07	0.002	0.0138	1.38	1					
	Barren	7821	1.01	1208	57.11	0.1544	0.9592	95.92	96					
	Forest	477828	61.45	145	6.85	0.0003	0.0018	0.188	1					
	Planted / Cultivated	177173	22.78	529	25.01	0.0029	0.0185	1.85	2					
Sum		777518	100	2115	100	0.1610				0.001	0.959	0.957	0.143	6.67
TWI	0-7	412450	83.48	1872	88.51	0.0045	0.3244	32.44	32					
	7.0-12	75017	15.18	217	14.57	0.0028	0.2067	20.67	20					
	12-17.0	6206	1.25	25	3.99	0.0040	0.2879	28.79	28					
	17-23	395	0.079	1	0.047	0.0025	0.1809	18.09	18					
Sum		494068		2115		0.013				0.180	0.324	0.143	0.143	1.00
Curvature	Concave	204502	41.52	1489	70.40	0.007	0.770	77	77					
	Convex	288026	58.47	626	29.59	0.002	0.229	22.9	23					
Sum		492528		2115		0.0094				0.229	0.770	0.540	0.143	3.77

In the Table 23 FR method use statistical models to quantify the relationship between landslide occurrences and the selected variables hence each raster cells of landslide is calculated with raster cells of each factor, So for frequency method the working environment of each cells should be same In the each classes of slope the slope in the range from 30 to 45 has maximum landslide pixels hence the frequency ratio is calculated from each landslide pixels after the frequency ratio is calculated then from the frequency ratio RF is calculated from RF the prediction rate is calculated. In the above table the prediction rate for Slope is 1.94. Similarly, Aspect is also another causative factor whose southern face has maximum landslide pixels; more than 60 percent of landslides are observed in this region. The prediction rate for aspect is 2.56. Moving forward to lithology, Chandragiri formation has maximum no of landslides and Phulchauki formation has no landslide encountered. In Chandragiri formation about 58 percent of landslides are found. The prediction rate for lithology is 2.82. Distance from the road is another factor here nearer the distance from road high is the percentage of landslide. Maximum landslide pixels of landslide are in a 0-1300-meter distance from the road; the prediction rate calculated for the road is 5.25. Distance from fault and drainage also shows similar pattern as of road i.e nearer the distance from fault higher is the landslide pixel percentages. In the case of distance from drainage, the maximum landslide pixel count of 1636 is found at a distance of 1000m from the drainage. In case of Distance from fault maximum landslide noted is in between 1300m. The prediction Rate for Drainage and Fault is 3.37 and 2.31. For Land use and land cover maximum landslide is in the Barren area as shown in Table 23 with the landslide pixel of 95%. The prediction rate for LULC is 6.67. Precipitation is another extrusive causative factor for landslide, maximum landslide is calculated to be in the class range of 1038mm - 1048 mm precipitation range. For the precipitation the prediction rate is 2.46. Also the two remaining factors TWI and curvature have prediction rates of 1 and 3.7. In TWI higher the classes fewer landslide pixel was noted. In Curvature concave class has a maximum landslide of 70%.

4.5.4 Landslide Susceptibility Map from Frequency Ratio Method:

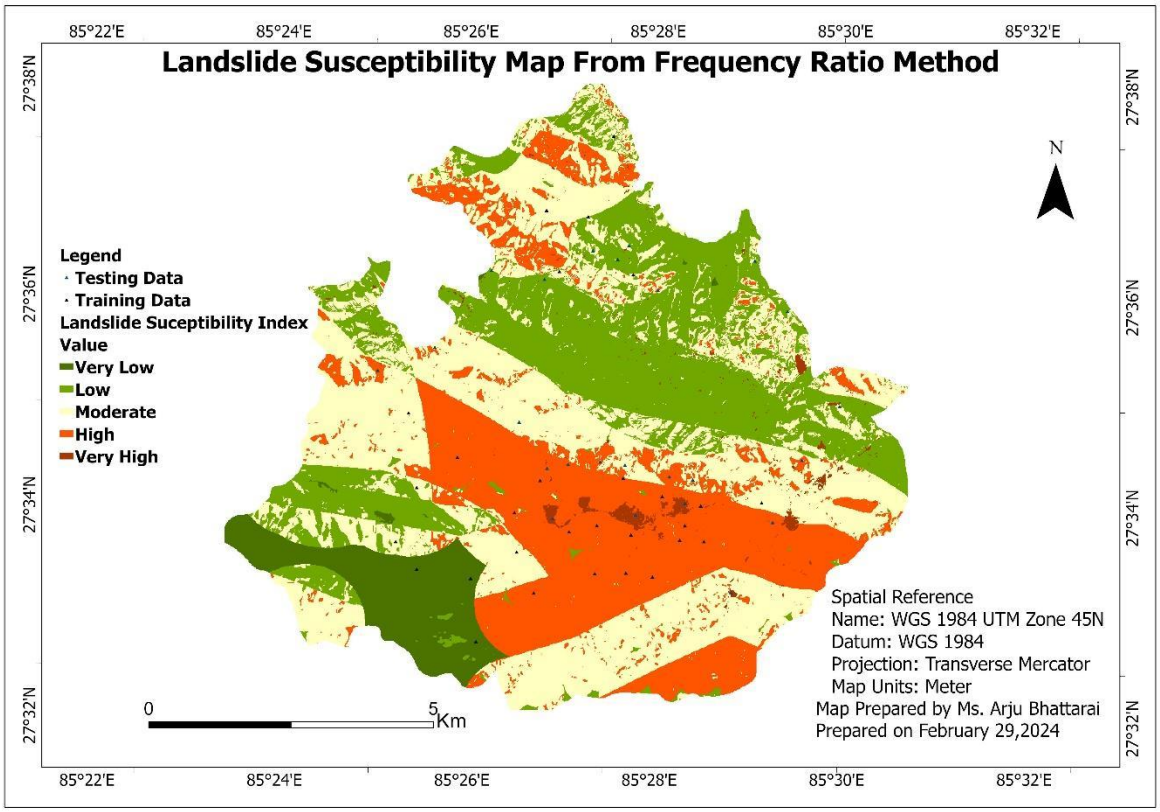

Figure 20: Landslide Susceptible Map from Frequency Ratio Method

LSM was accomplished using the Frequency Ratio approach as shown in Figure 20. Frequency Ratio was used to weight factors and classes. Raster maps of each factor were weighted on a cell-by-cell basis. The integration of the weighted raster map produced an LSM map containing numerical susceptibility data, with higher LSI values indicating high susceptibility and lower values indicating low susceptibility. LSI values vary from 356- 1864. Now the distribution of landslide susceptibility zones and landslide occurrence is given in Table 24

Table 24: The distribution of landslide susceptibility zones and landslide occurrence.

LSI	LSI Pixel	LSI %	Landslide Pixel	Landslide%	Landslide Area(m2)
Very Low	34256	6.94	8	0.37	1250
Low	132040	26.76	166	7.84	25937.5
Moderate	188324	38.17	277	13.09	43281.25
High	133788	27.12	452	21.37	70625
Very High	4993	1.01	1212	57.30	189375
Sum	493401		2115		

In the Table 24 maximum class percentage of 38.17 is in moderate zone, 1.01 which least percentage is observed in very high zone.

4.5.5 Comparison Based on Landslide Density

Landslide density is the ratio of area of an existing landslide to the area of each landslide susceptibility class. In the present study, it is calculated on the basis of the number of pixels. In an ideal landslide susceptibility map, the high susceptibility zone should have the highest landslide density and there should be a decreasing trend of the density values successively from medium to low susceptibility zones. The landslide densities of the susceptibility classes of both the LSM maps are calculated and tabulated in the Table 25.

Table 25: The landslide densities of the susceptibility classes of both the LSM maps

	Frequency Ratio Method			Analytical Hierarchical Process Method		
LSI	**Class Pixel**	**Landslide Pixel**	**Density**	**Class Pixel**	**Landslide Pixel**	**Density**
Very Low	34256	8	0.0002	7532	9	0.0012
Low	132040	166	0.0013	137632	144	0.001
Moderate	188324	277	0.0015	258261	530	0.0021
High	133788	452	0.0034	87568	1253	0.0143
Very High	4993	1212	0.2427	2408	179	0.0743
Sum	493401	2115		493401	2115	

In the above Table 25 for FR, Very Low LSI class, there are 34,256 pixels, and the density of landslide pixels is 0.0002. This means that out of the total pixels classified in the Very Low LSI class, only a very small proportion (0.02%) are identified as landslide pixels. For AHP, the Very Low LSI class, there are 7532 pixels, and the density of landslide pixels is 0.0012. This means that out of the total pixels classified in the Very Low LSI class, a small proportion (0.12%) are identified as landslide pixels.

4.5.5 Validation of FR and AHP method

There are various methods to check the validity of the LSM map, in this study AUC/ROC curve is used, and ROC curve methods rely on incorrectly classified data. Landslide zones (false positives) and incorrectly identified non-landslide areas (false negatives), with a prediction rate. The curve method depends on training and testing landslides i.e. existing landslides,

was used to validate the accuracy of the landslide susceptibility map. In Figure 21 AUC value 0.7547 is achieved for the present model which can be converted in terms of a percent success rate accuracy of 75.47%. So it can be said that the AHP model gave an accuracy of 75.47%. Additionally, in Figure 22 AUC value achieved is 0.852. Hence it could be said that the FR model has a high accuracy of 85.2% in comparison to the AHP approach.

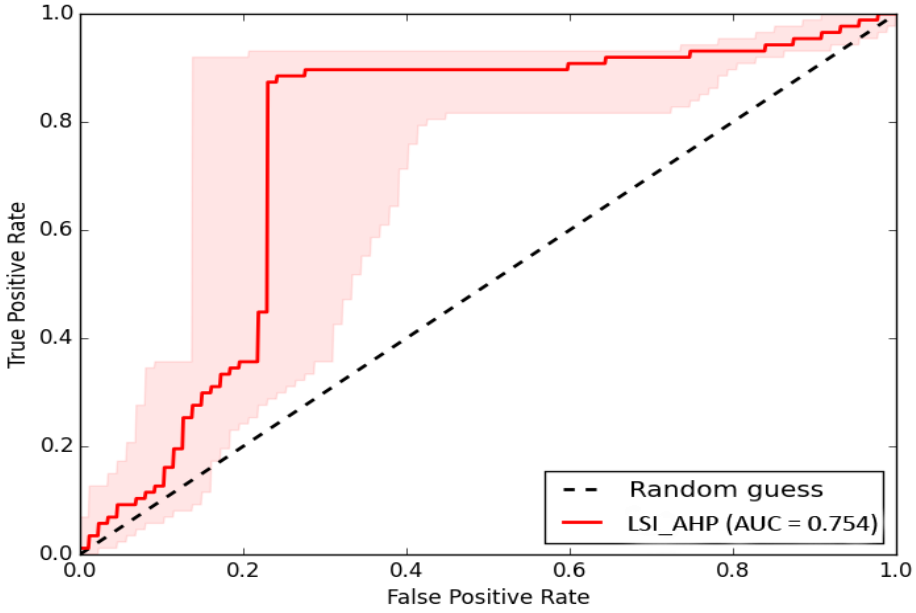

Figure 21: AUC Curve for validation of Map from AHP method

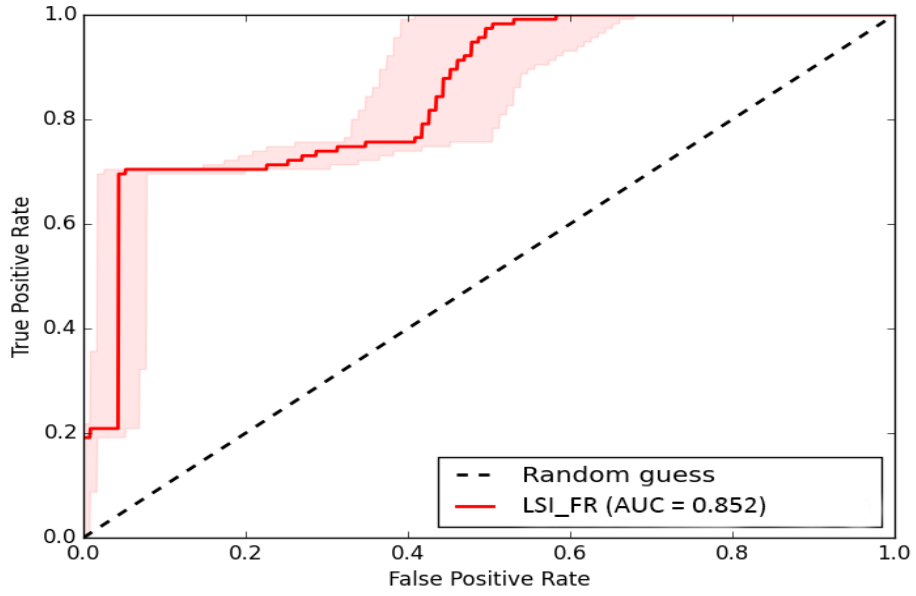

Figure 22: AUC Curve for validation of Map from Frequency Ratio method

CHAPTER 5: Discussions

The study aimed to identify elements that cause landslides, create a susceptibility map using a geographic information system, and monitor changes using remote sensing techniques. With the help of LSM map planner determines acceptable or unacceptable risk levels for development plans. Decisions can be made to avoid, prevent, or mitigate landslide hazards in the development program. Choosing the landslide causative parameters is the first and most important step when developing a landslide susceptibility map. In Sindhupalchwok for LSM 12 causative factors contributing to landslides were considered, including slope, aspect, elevation, geology, land use, proximity to roads and drainage, plan curvature, profile curvature, NDVI (Normalized Difference Vegetation Index), soil type and rainfall (Pradhan & Dahal, 2023). However in this study area 10 causative factors were used for producing LSM. In this study area, it has been discovered that slope is the most important characteristic influencing landslide susceptibility, and the high and very high susceptibility classes on the weight of evidence modeled susceptibility map correspond to steeply sloped terrain (30°-45°). In South Africa also this is no surprise, as slopes greater than 18° are considered to be susceptible to landslides, and therefore not suitable for construction (Boelhouwers J et al., 1998. South facing slopes have long been known to be more susceptible to landslides (Boelhouwers J et al., 1998). This was further confirmed in this study when the South facing slopes recorded the highest number of landslides.

Landslides are influenced by the area's geology, as different rock types have varying hydrological qualities and strength levels. Geological structures can weaken rocks. It has been noted by (Dahal et al., 2014) lithology is also a major causative factor for inducing landslides. In the result of the study area Chandragiri formation has the maximum landslide area, the prominent rock found in that area is limestone. Limestone has a high hydraulic transmissivity; higher transmissivity allows water to penetrate deeper into the ground, leading to decreased cohesive strength of clay minerals and higher pore fluid pressure (Warrick AW et al., 1977). (Dahal et al., 2014) also suggest Landslides are more prone to occur in locations with faults and lithological connections due to their inherent vulnerability. In the study area the fault distance from 0-1300 consists of maximum landslide pixel. The road network exhibits high and extremely high susceptibility classes in the LSM (Kumar & Anbalagan, 2016). In this study the maximum landslides were analyzed to be near road i.e.0-1300m. In the LSM map in Tehri region Uttarakhand by (Kumar & Anbalagan, 2016) the results also showed that highly

vulnerable classes occupied regions near the drainage network. Low susceptibility classes are seen in locations with flat terrain, high forest cover, and sparse forest cover. Settlement areas have been classified as somewhat to moderate to highly susceptible. The LSM map from this research also provides similar results: few landslides are seen in forest regions and moderate chances of susceptibility are seen in built up areas. Barren slopes are more susceptible to landslides based on field observations and in LULC map also we could see a maximum number of landslides occurring in barren areas. Slope curvature as a factor Dahal, 2014 suggests curvatures, along with other parameters, influence water flow in and out of slopes, making them crucial for studying landslides. In this study also maximum landslides above 60% percent were analyzed to be in concave curvature. The Topographic Wetness Index is a parameter used in terrain analysis to estimate the relative wetness or moisture content of the land surface. It is calculated based on topographic characteristics such as slope and flow accumulation in this study area lower the value of TWI higher the landslide was observed. Maximum landslides were observed in class 0-7 and the Landslide percentage decreases higher the value of TWI.

Properly understanding and selecting the landslide causative elements leads to more accurate landslide susceptibility modeling. The accuracy of the landslide susceptibility map relies on weighing the causative characteristics based on their impact on slope instability. Therefore, selecting an appropriate weighting system was crucial in this work. This study utilized both the weight of evidence and the map combination approach. There are 34,256 pixels in the FR Very Low LSI class, and the density of landslide pixels is 0.0002. This indicates that just a very tiny percentage (0.02%) of all pixels classified in the Very Low LSI class are identified as landslide pixels. There are 7532 pixels in the Very Low LSI class AHP, and the density of landslide pixels is 0.0012. This indicates that a tiny percentage (0.12%) of all the pixels classified in the Very Low LSI class are landslide pixels. The analysis revealed a Prediction Rate (PR) of 9.35 for 'Land use', the highest among all factors considered (Pradhan & Dahal, 2023). In this study area also it is revealed similar maximum prediction rate of 6.67 for LULC from FR method. The difference is seen in the final map too because both are different techniques; one includes weightage whereas another is dependent on the raster cell size of landslides and its factors However, the Frequency Ratio method outperformed the AHP method in this analysis. The ROC/AUC curve suggests that the accuracy of AHP is about 75% in contrast to the FR which is about 85%. Total 138 landslides were observed in the study area and plotted into polygons among them 70 percent were

distinguished as training datasets whereas 30 percent as testing data sets. Testing data sets were used in plotting AUC curves.

5.1 Pros and Cons of FR and AHP method

The AHP decision-making method considers several criteria and perspectives, resulting in a thorough evaluation (Saaty, 2001). This technique offers an organized approach to decision-making, ensuring consistent and dependable evaluations. AHP weights criteria based on their relative value, prioritizing key aspects in decision-making. AHP additionally provides for the incorporation of expert opinion, providing valuable insights and perspectives to the evaluation process which totally depends upon the weightage given by a person is the huge drawback of AHP Method.

The FR approach is simple and straightforward to use, requiring easily available data. This method can determine the most relevant factors for landslide occurrence by examining their frequency distribution and link to landslide incidents. It is suitable for vast areas since it employs statistical analysis of previous landslide events to identify areas prone to landslides. However, this technique is skewed toward places with previous landslides and may be inaccurate in areas without such incidents. The FR method's accuracy is limited because it is based on previous landslide incidents and the availability of accurate data. The FR method is a statistical approach that does not include the physical factors that lead to landslide occurrence. The FR method assumes that the influence of conditioning factors on landslide occurrence is consistent across the entire study area, which may not be accurate in reality (Ehret et al., 2010).

5.2 Recommendation

The susceptibility of the area to landslides is critical for development planning. Landslides can disrupt human activity and have a negative impact on the economy. In this sense, understanding the area's susceptibility to landslides is critical. Landslide susceptibility maps can only show regions that are likely to have landslides, not when the landslides will occur.

Before creating a landslide susceptibility map, it's necessary to conduct a detailed inventory and classification of the slides. Researchers can create susceptibility maps for rock falls, debris flows, and deep landslides. This is important because other variables, such as road cuts, have a greater impact on rock falls.

The planner can use these estimations to make decisions about the site's suitability, the type of development, and the relevant mitigation measures. Final LSM map have 5 classes with the range of susceptibility from very low to very high. This map would be very helpful for planning of construction of parks and paragliding in Nagi dada Mitigating failures involves implementing measures to enhance slope stability and reduce the risk of detachment and movement along wedge-shaped planes. Here are some common mitigation measures for addressing all the failures (Popescu & Sasahara, 2009):

1. **Slope Geometry Modification:** Adjusting the slope geometry can be an effective mitigation strategy. This may include reducing the slope angle or altering the overall slope configuration to minimize the potential for wedge formation.
2. **Surface Water Management:** Proper drainage is crucial for slope stability. Managing surface water through the installation of drainage systems, such as surface ditches, subsurface drains, or retaining walls, helps prevent water infiltration and the development of pore water pressure within the slope that can contribute to wedge failures.
3. **Vegetative Cover:** Establishing and maintaining vegetation on slopes can improve stability by reducing surface erosion, enhancing soil cohesion, and absorbing water. The roots of plants provide additional reinforcement to the soil, contributing to slope stability.
4. **Rock Bolting and Reinforcement:** In areas prone to wedge failures, reinforcing the slope with rock bolts or soil nails can help stabilize the material and prevent detachment along potential failure planes. Reinforcement materials are often inserted into the slope to increase cohesion and shear strength.
5. **Slope Monitoring and Early Warning Systems:** Implementing monitoring systems, such as inclinometers, piezometers, or geotechnical sensors, can help detect early signs of slope movement. Early warning systems allow for timely alerts, enabling precautionary measures and evacuation if necessary.
6. **Retaining Structures:** Constructing retaining walls or other engineered structures can provide additional support to slopes susceptible to wedge failures. These structures can help redistribute the lateral forces acting on the slope and resist potential sliding.
7. **Geotechnical Investigations:** Thorough geotechnical investigations are essential for understanding the subsurface conditions, identifying potential failure planes, and designing appropriate mitigation measures. This may involve soil testing, geophysical surveys, and other site-specific assessments.

8. **Public Awareness and Land Use Planning:** Informing the public about potential landslide hazards and implementing proper land use planning can help avoid development in high-risk areas. Zoning regulations and building codes can be designed to limit construction on unstable slopes.

CHAPTER 6: Conclusions

LSM was accomplished using the AHP and FR approach. AHP was used to weight factors and their classifications. The weight values have been given to each factor's raster maps on a cell-by-cell basis in FR method and for AHP method multiple literature review, field work and consultation with expertise weightage was given to each factor. Integration of weightage to each factor produced an LSI map with numerical susceptibility information, where larger values indicate high susceptibility and lower values indicate low susceptibility. The LSI from AHP method values vary from 6.58 to 37 Similarly, LSI value ranges from 356- 1864. The continuous LSI map from both the methods was divided into five groups using the natural break classifier. There are five levels of susceptibility: very low, low, moderate, high, and extremely high. From the result of both the map maximum region of the study area has moderate chances of landslide i.e. about 58 percentage of the study area is susceptible of Landslide from AHP in contradict to FR method about 48 percentages is of total area has moderate chances similarly in FR method 27 percentage of area is susceptible to landslide whereas AHP method provides 22 percentage of predication. However, the map presented by AHP and FR both is recommendable because the success rate of AHP is about 75% and FR is 85%.

The first stage in planning for future land use is to assess the requirement for landslide susceptibility information to avoid exceeding an acceptable level of risk. Landslide risk refers to the degree of loss caused by a certain landslide. Landslide information aims to identify regions vulnerable to landslides and recommend appropriate development measures. Landslides can disrupt human activities and the economy. Understanding the area's landslide risk is vital. Landslide susceptibility maps only show locations with a high likelihood of landslides, not when they may occur. Planners can use these estimations to make decisions about site suitability, kind of development, and mitigation measures.

References:

Abdo, H. G. (2022). Assessment of landslide susceptibility zonation using frequency ratio and statistical index: A case study of Al-Fawar basin, Tartous, Syria. *International Journal of Environmental Science and Technology*, *19*(4), 2599–2618. https://doi.org/10.1007/s13762-021-03322-1

Abedini, M., & Ghasemyan. (2017). .Landslide susceptibility mapping in Bijar city, Kurdistan Province, Iran: A comparative study by logistic regression and AHP models. Environmental earth sciences, 76, 1-14. *Environmental Earth Sciences, 76, 1-14.*

Bera, A., Mukhopadhyay, B. P., & Das, D. (2019). Landslide hazard zonation mapping using multi-criteria analysis with the help of GIS techniques: A case study from Eastern Himalayas, Namchi, South Sikkim. *Natural Hazards*, *96*(2), 935–959. https://doi.org/10.1007/s11069-019-03580-w

Bhandari, R.K., Upreti, & B.N. (2015). Geological investigation of landslides in the northern part of Kavrepalanchok District, Central Nepal. *Journal of Nepal Geological Society, 49, 15-22*.

Boelhouwers J, Duiker JMC, & van Duffelen EA. (1998). Spatial, morphological and sedimentological aspects of recent debris flows in Du Toit's Kloof. *African Journal of Geology. Vol. 101, Pp.73–89.*

Borrelli, L., Ciurleo, M., & Gullà, G. (2018). Shallow landslide susceptibility assessment in granitic rocks using GIS-based statistical methods: The contribution of the weathering grade map. *Landslides*, *15*(6), 1127–1142. https://doi.org/10.1007/s10346-018-0947-7

Chang, Z., Catani, F., Huang, F., Liu, G., Meena, S. R., Huang, J., & Zhou, C. (2023). Landslide susceptibility prediction using slope unit-based machine learning models considering the heterogeneity of conditioning factors. *Journal of Rock Mechanics and*

Geotechnical Engineering, *15*(5), 1127–1143. https://doi.org/10.1016/j.jrmge.2022.07.009

Cruden, C., & D.M. (1991). *A simple definition of a landslide* (Vol. 43). Bulletin of the International Association of Engineering Geology.

Cruden, Vranes, D.M., & D.J. (1996). Landslide Types and Processes, Special Report,. *Transportation Research Board, National Academy of Sciences, 247:36-75*.

Dahal, R. K. (2014). Regional-scale landslide activity and landslide susceptibility zonation in the Nepal Himalaya. *Environmental Earth Sciences*, *71*(12), 5145–5164. https://doi.org/10.1007/s12665-013-2917-7

Dai, F. C., Lee, C. F., & Ngai, Y. Y. (2002). Landslide risk assessment and management: An overview. *Engineering Geology*.

Dhungana, G., Ghimire, R., Poudel, R., & Kumal, S. (2023). Landslide susceptibility and risk analysis in Benighat Rural Municipality, Dhading, Nepal. *Natural Hazards Research*, *3*(2), 170–185. https://doi.org/10.1016/j.nhres.2023.03.006

Duncan, J. M. (1996). LANDSLIDES: INVESTIGATION AND MITIGATION. CHAPTER 13 - SOIL SLOPE STABILITY ANALYSIS. *Transportation Research Board Special Report*, *247*. https://trid.trb.org/View/462511

Ehret, D., Rohn, J., Dumperth, C., Eckstein, S., Ernstberger, S., Otte, K., Rudolph, R., Wiedenmann, J., Xiang, W., & Bi, R. (2010). Frequency ratio analysis of mass movements in the Xiangxi catchment, Three Gorges Reservoir area, China. *Journal of Earth Science*, *21*(6), 824–834. https://doi.org/10.1007/s12583-010-0134-9

El Jazouli, A, Barakat, Khellouk, & R. (2019). GIS-multicriteria evaluation using AHP for landslide susceptibility mapping in Oum ER Rbia high basin (Morocco). Geoenvironmental Disasters, 6(1). *Geoenvironmental Disasters, 6(1).* https://doi.org/10.1186/s40677-019 0119-7

Fall, M., Azzam, R., & Noubactep, C. (2006). A multi-method approach to study the stability of natural slopes and landslide susceptibility mapping. *Engineering Geology*, *82*(4), 241–263. https://doi.org/10.1016/j.enggeo.2005.11.007

Geest, K. V. D., & Schindler, M. (n.d.). *CASE STUDY REPORT: LOSS AND DAMAGE FROM A CATASTROPHIC LANDSLIDE IN SINDHUPALCHOK DISTRICT, NEPAL*.

Gerrard, J, Gardner, & R. (n.d.). *Relationships between landsliding and land use in the Likhu Khola drainage basin, Middle Hills, Nepal.* Mountain Research and Development, 22, pp. 48-55.

Ghosh, S., Kumar, A., & Bora, A. (2014). Analyzing the stability of a failing rock slope for suggesting suitable mitigation measure: A case study from the Theng rockslide, Sikkim Himalayas, India. *Bulletin of Engineering Geology and the Environment*, *73*(4), 931–945. https://doi.org/10.1007/s10064-014-0586-8

Gokceoglu, M. E., Candan. (2002). Assessment of landslide susceptibility for a landslide-prone area (north of Yenice, NW Turkey) by fuzzy approach. *Environmental Geology*, *41*(6), 720–730. https://doi.org/10.1007/s00254-001-0454-2

Gupta, N., Pal, S. K., & Das, J. (2022). GIS-based evolution and comparisons of landslide susceptibility mapping of the East Sikkim Himalaya. *Annals of GIS*, *28*(3), 359–384. https://doi.org/10.1080/19475683.2022.2040587

Guzzetti, F., Reichenbach, P., Cardinali, M., Galli, M., & Ardizzone, F. (2005). Probabilistic landslide hazard assessment at the basin scale. *Geomorphology*, *72*(1–4), 272–299. https://doi.org/10.1016/j.geomorph.2005.06.002

Hasegawa, S., Dahal, R. K., Yamanaka, M., Bhandary, N. P., Yatabe, R., & Inagaki, H. (2009). Causes of large-scale landslides in the Lesser Himalaya of central Nepal. *Environmental Geology*, *57*(6), 1423–1434. https://doi.org/10.1007/s00254-008-1420-z

Hasekioğulları, G. D., & Ercanoglu, M. (2012). A new approach to use AHP in landslide susceptibility mapping: A case study at Yenice (Karabuk, NW Turkey). *Natural Hazards*, *63*(2), 1157–1179. https://doi.org/10.1007/s11069-012-0218-1

Hoo, Z. H., Candlish, J., & Teare, D. (2017). What is an ROC curve? *Emergency Medicine Journal*, *34*(6), 357–359. https://doi.org/10.1136/emermed-2017-206735

Kanungo, D. P., Arora, M. K., Sarkar, S., & Gupta, R. P. (2009). A fuzzy set based approach for integration of thematic maps for landslide susceptibility zonation. *Georisk: Assessment and Management of Risk for Engineered Systems and Geohazards*, *3*(1), 30–43. https://doi.org/10.1080/17499510802541417

Kayastha, P., Dhital, M. R., & De Smedt, F. (2013). Application of the analytical hierarchy process (AHP) for landslide susceptibility mapping: A case study from the Tinau watershed, west Nepal. *Computers & Geosciences*, *52*, 398–408. https://doi.org/10.1016/j.cageo.2012.11.003

Kumar, R., & Anbalagan, R. (2016). Landslide susceptibility mapping using analytical hierarchy process (AHP) in Tehri reservoir rim region, Uttarakhand. *Journal of the Geological Society of India*, *87*(3), 271–286. https://doi.org/10.1007/s12594-016-0395-8

Li, T, Wang, & S. (1992). Landslide Hazards and their Mitigation in China. *Science Press, Beijing, 84 Pp.*

McAdoo, B. G., Quak, M., Gnyawali, K. R., Adhikari, B. R., Devkota, S., Rajbhandari, P. L., & Sudmeier-Rieux, K. (2018). Roads and landslides in Nepal: How development affects environmental risk. *Natural Hazards and Earth System Sciences*, *18*(12), 3203–3210. https://doi.org/10.5194/nhess-18-3203-2018

Mohammady, M., Pourghasemi, H. R., & Pradhan, B. (2012). Landslide susceptibility mapping at Golestan Province, Iran: A comparison between frequency ratio,

Dempster–Shafer, and weights-of-evidence models. *Journal of Asian Earth Sciences*, *61*, 221–236. https://doi.org/10.1016/j.jseaes.2012.10.005

Mondal, S., & Maiti, R. (2013). Integrating the Analytical Hierarchy Process (AHP) and the frequency ratio (FR) model in landslide susceptibility mapping of Shiv-khola watershed, Darjeeling Himalaya. *International Journal of Disaster Risk Science*, *4*(4), 200–212. https://doi.org/10.1007/s13753-013-0021-y

Moradi, M., Bazyar, M. H., & Mohammadi, Z. (2012). *GIS-Based Landslide Susceptibility Mapping by AHP Method, A Case Study, Dena City, Iran*.

Mr. Digvijay P. Salunkhe, Assist. Prof. Guruprasd Chvan, Ms. Rupa N. Bartakke, Ms. Pooja R Kothavale, & Kit's college of engineering, Kolhapur. (2017). An Overview on Methods for Slope Stability Analysis. *International Journal of Engineering Research And*, *V6*(03), IJERTV6IS030496. https://doi.org/10.17577/IJERTV6IS030496

Panauti Municipality. (2024). *Brief Introducation*. https://panautimun.gov.np/en

Panchauri, A., & Pant, M. (1992). P Landslide hazard mapping based ongeological attributes. *Eng Geol 32:81–100*.

Paudel, P. N., & Tamrakar, N. K. (2013). Geology and rockmass condition of Dhulikhel-Panchkhal area, Kavre District, Central Nepal Lesser Himalaya. *Bulletin of the Department of Geology*, *15*, 1–14. https://doi.org/10.3126/bdg.v15i0.7412

Petley, D. N., Hearn, G. J., Hart, A., Rosser, N. J., Dunning, S. A., Oven, K., & Mitchell, W. A. (2007). Trends in landslide occurrence in Nepal. *Natural Hazards*, *43*(1), 23–44. https://doi.org/10.1007/s11069-006-9100-3

Popescu, M. E., & Sasahara, K. (2009). Engineering Measures for Landslide Disaster Mitigation. In K. Sassa & P. Canuti (Eds.), *Landslides – Disaster Risk Reduction* (pp. 609–631). Springer Berlin Heidelberg. https://doi.org/10.1007/978-3-540-69970-5_32

Rahman, G., Bacha, A. S., Ul Moazzam, M. F., Rahman, A. U., Mahmood, S., Almohamad, H., Al Dughairi, A. A., Al-Mutiry, M., Alrasheedi, M., & Abdo, H. G. (2022).

Assessment of landslide susceptibility, exposure, vulnerability, and risk in shahpur valley, eastern hindu kush. *Frontiers in Earth Science*, *10*, 953627. https://doi.org/10.3389/feart.2022.953627

Roccati, A., Paliaga, G., Luino, F., Faccini, F., & Turconi, L. (2021). GIS-Based Landslide Susceptibility Mapping for Land Use Planning and Risk Assessment. *Land*, *10*(2), 162. https://doi.org/10.3390/land10020162

Rusydy, Al-Huda, Fahmi, & Effendi. (2019). Kinematic Analysis and Rock Mass Classifications for Rock Slope Failure at USAID Highways. *SDHM Structural Durability and Health Monitoring*, *13*, 378–398. https://doi.org/10.32604/sdhm.2019.08192

Saaty, T.L., Vargas, & L.G. (2001). *The Seven Pillars of the Analytic Hierarchy Process. Models, Methods, Concepts & Applications of the Analytic Hierarchy Process, 27–46.*

Sarkar, S., & Kanungo, D. P. (2004). An Integrated Approach for Landslide Susceptibility Mapping Using Remote Sensing and GIS. *Photogrammetric Engineering & Remote Sensing*, *70*(5), 617–625. https://doi.org/10.14358/PERS.70.5.617

Shahabi, H., & Hashim, M. (2015). Landslide susceptibility mapping using GIS-based statistical models and Remote sensing data in tropical environment. *Scientific Reports*, *5*(1), 9899. https://doi.org/10.1038/srep09899

Siwakoti, & D.R. (2000). *An assessment of soil loss and natural hazards in Nepal.* Journal of Nepal Geological Society 21,41-48. DOI:10.3126/jngs.v21i0.32150

Stöcklin, & Bhattarai. (1977). *Geology of Kathmandu area and Central Mahabharat range: Nepal Himalaya.*

Tehrany, M. S., Pradhan, B., & Jebur, M. N. (2015). Flood susceptibility analysis and its verification using a novel ensemble support vector machine and frequency ratio method. *Stochastic Environmental Research and Risk Assessment*, *29*(4), 1149–1165. https://doi.org/10.1007/s00477-015-1021-9

Vakhshoori, V., & Zare, M. (2018). Is the ROC curve a reliable tool to compare the validity of landslide susceptibility maps? *Geomatics, Natural Hazards and Risk*, *9*(1), 249–266. https://doi.org/10.1080/19475705.2018.1424043

Varnes, & D.J. (n.d.). *Slope movements: Types and processes.* In: Schuster, R.L. and Krizek, R.J. (eds.)Landslide analysis and control, National Academy of Sciences, Transportation Research Board Special Report 176, Washington, 11-33.

Warrick AW, Mullen GJ, & Nielsen DR. (1977). .Scaling field measured soil hydraulic properties using a similar media concept. *Water Resource. Res. Vol. 13 (2), Pp. 355-362.*

Yalcin, A. (2007). Environmental Impacts of Landslides: A Case Study from East Black Sea Region, Turkey. *Environmental Engineering Science*, *24*(6), 821–833. https://doi.org/10.1089/ees.2006.0161

Yalcin, A. (2008). GIS-based landslide susceptibility mapping using analytical hierarchy process and bivariate statistics in Ardesen (Turkey): Comparisons of results and confirmations. *CATENA*, *72*(1), 1–12. https://doi.org/10.1016/j.catena.2007.01.003

Yalcin, A., Reis, S., Aydinoglu, A. C., & Yomralioglu, T. (2011). A GIS-based comparative study of frequency ratio, analytical hierarchy process, bivariate statistics and logistics regression methods for landslide susceptibility mapping in Trabzon, NE Turkey. *CATENA*, *85*(3), 274–287. https://doi.org/10.1016/j.catena.2011.01.014

Pradhan, P., & Dahal, B. K. (2023). Landslide Susceptibility Analysis of Jugal Rural Municipality, Sindhupalchok. *Journal of Science and Engineering*, *10*, 49–57. https://doi.org/10.3126/jsce.v10i1.61019

Annexes

Annexes- 1

Slope kinematics analysis

Location 1

S.N.	Dip	Dip Direction
1	55	230
2	30	158
3	68	100
4	86	341
5	67	180
6	45	38
7	31	176
8	77	247
9	36	129
10	7	72
11	81	340
12	79	220
13	47	178
14	24	200
15	21	210
16	34	200
17	41	134
181	60	210
19	65	109
20	26	198
21	43	210
22	67	167
23	76	345
24	54	178
25	81	240
26	55	49
27	34	76
28	41	157
29	31	215
30	21	317
31	60	180
32	65	200
33	56	340
34	43	267

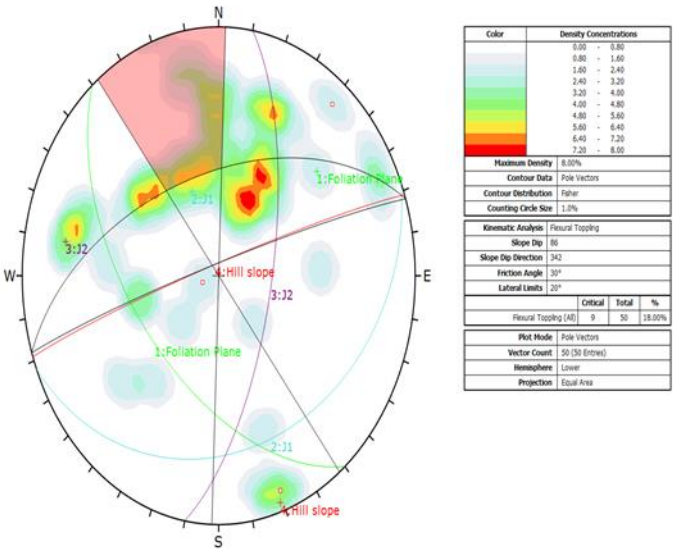

35	44	134
36	34	144
37	36	164
38	56	199
39	58	108
40	43	211
41	22	45
42	34	78
43	77	169
44	34	222
45	47	95
46	67	100
47	42	198
48	60	200
49	39	180
50	44	120

Location 2

S.N.	Dip	Dip Direction
1	76	320
2	70	60
3	65	74
4	86	38
5	69	100
6	20	120
7	35	300
8	27	260
9	46	76
10	66	279
11	56	188
12	55	350
13	33	120
14	76	147
15	56	70
16	54	98
17	37	100
181	68	128
19	42	133
20	67	254
21	39	89
22	56	90

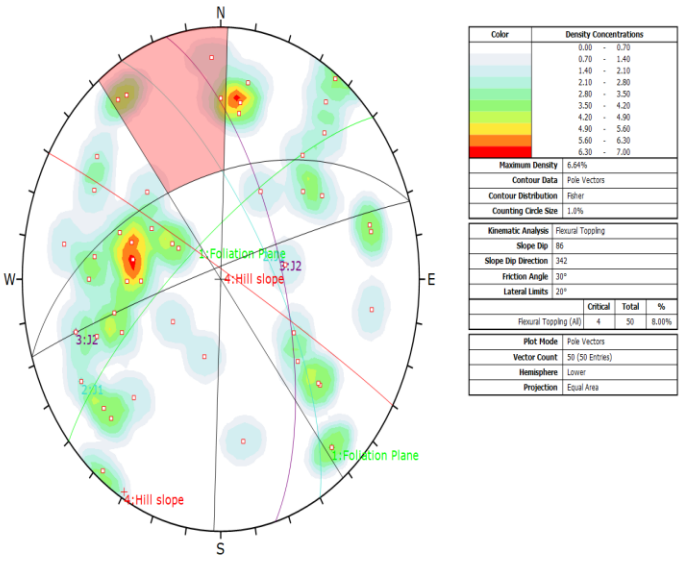

23	45	110
24	76	320
25	67	256
26	54	310
27	24	55
28	67	45
29	33	89
30	77	177
31	51	237
32	67	222
33	67	49
34	54	43
35	23	120
36	77	144
37	88	216
38	45	230
39	39	108
40	42	310
41	61	180
42	33	210
43	45	67
44	26	15
45	68	190
46	54	220
47	55	310
48	60	188
49	62	119
50	77	217

S.N.	Dip	Dip Direction
1	80	330
2	73	55
3	69	62
4	87	30
5	41	230
6	24	90
7	31	180
8	67	275
9	58	66
10	49	57
11	78	195

12	67	220
13	56	170
14	67	220
15	77	147
16	38	247
17	55	330
181	78	98
19	76	100
20	67	192
21	54	201
22	34	67
23	44	78
24	43	89
25	33	138
26	45	270
27	54	180
28	45	197
29	87	200
30	88	300
31	68	267
32	43	301
33	43	308
34	39	321
35	56	88
36	58	66
37	43	15
38	12	160
39	45	247
40	56	210
41	33	89
42	31	210
43	48	331
44	67	195
45	66	348
46	56	34
47	87	198
48	45	200
49	44	215
50	68	345
	54	176
	43	96

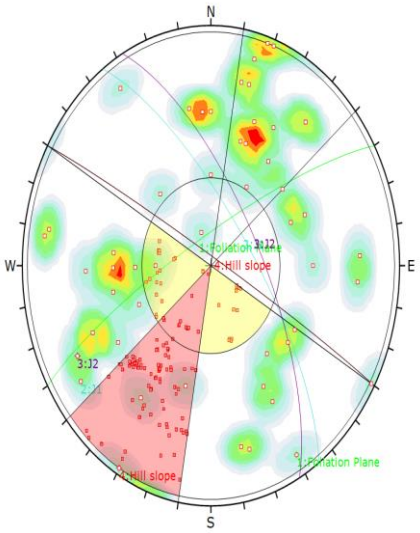

Symbol	Feature
	Critical Intersection

Color	Density Concentrations
	0.00 - 0.60
	0.60 - 1.20
	1.20 - 1.80
	1.80 - 2.40
	2.40 - 3.00
	3.00 - 3.60
	3.60 - 4.20
	4.20 - 4.80
	4.80 - 5.40
	5.40 - 6.00

Maximum Density	5.84%
Contour Data	Pole Vectors
Contour Distribution	Fisher
Counting Circle Size	1.0%

Kinematic Analysis	Direct Toppling
Slope Dip	87
Slope Dip Direction	30
Friction Angle	30°
Lateral Limits	20°

	Critical	Total	%
Direct Toppling (Intersection)	118	1324	8.91%
Oblique Toppling (Intersection)	34	1324	2.57%
Base Plane (All)	4	52	7.69%

Plot Mode	Pole Vectors
Vector Count	52 (52 Entries)
Intersection Mode	Grid Data Planes
Intersections Count	1324
Hemisphere	Lower
Projection	Equal Area

Annexes-2

Rainfal Data

Sum of Godavari(Sum) Row Labels	Column Labels January	February	March	April	May	June	July	August	September	October	November	December	Grand Total
2010	4.4	22	0.4	49	89.5	173.1	337.3	353.9	0	75.2	0	0	1104.8
2011	4.2	47.6	27.7	62.5	345.2	402.6	417.8	399.1	298.4	0	0	0	2005.1
2012	20.2	38.8	3.1	89	51.8	118.4	503.8	371.2	2.7	0	0	0	1199
2013	16.3	58.8	17.8	52.7	256	367.1	489.6	351.2	234.3	123.4	0	0	1967.2
2014	2.6	27	36.7	11.1	106.4	70.8	493.6	338.2	209.4	96.4	0	18.7	1410.9
2015	0.7	38.4	94.5	112.1	30.9	123.6	291.1	332.5	171.3	23.7	0	0	1218.8
2016	7.8	9.8	1.6	3.4	119.4	174.7	525.4	377.6	225.6	29	0	0	1474.3
2017	21	0	70.7	65	104.7	149.1	354.3	421.3	143.4	5.4	0	0	1334.9
2018	5.8	1.9	7.5	33.8	70.1	238.7	412	554.1	77.4	0	0	0	1401.3
2019	27.5	84.3	42.6	81.1	109.2	76.1	631.9	291.9	294.4	7.7	0	26.2	1672.9
2020	89.6	25.4	26.4	190.8	126	352.5	525.6	215.1	217.6	0	0	0	1769
2021	0	9.2	4.9	93.1	187.9	245.6	537.5	378.11	206.9	41	0	50.2	1754.41
2022	8.2	55.8	1.5	74.8	235.3	343	305.9	274.5	150.9	136.7	0	0	1586.6
Grand Total	**208.3**	**419**	**335.4**	**918.4**	**1832.4**	**2835.3**	**5825.8**	**4658.71**	**2232.3**	**538.5**	**0**	**95.1**	**19899.21**
Average	16.02307692	32.2308	25.8	70.65	140.95	218.1	448.14	358.362	171.7154	41.423	0	7.315385	1530.7085

Sum of Nangkhel(Sum) Row Labels	Column Labels January	February	March	April	May	June	July	August	September	October	November	December	Grand Total
2010	0	26.4	14.8	91.6	41.5	90.8	290.3	416.2	204.6	32.4	0	0	1208.6
2011	3.8	45.5	12.7	55.2	189.5	245.8	372.4	360.5	268.1	9.9	36.1	0	1599.5
2012	10.2	28.9	12.4	67.3	23.7	135.3	352.3	291.2	249.8	8.3	0	0	1179.4
2013	11	40.1	17	49.4	168.9	176.3	391.4	291.6	121.5	93.5	0	0	1360.7
2014	2.1	16.4	62.9	9.7	138.1	110.4	337.7	332.4	229.9	118.1	0	16.7	1374.4
2015	4.2	32.5	79.3	78.7	66.6	101.2	258.3	571	133.7	41	0	0	1366.5
2016	1.2	6.2	0	12.5	122.7	279.8	434.5	142.1	119.1	82.3	0	0	1200.4
2017	17.7	0	0	72	142.8	145.4	295	300.3	139.6	18	0	0	1130.8
2018	9.5	3.5	44	120.1	88.5	133.4	371.1	422.4	83.3	5	0	0	1280.8
2019	17.9	80.7	36.4	106.6	77.6	147.2	459.5	258.8	219.5	6.8	0	20.2	1431.2
2020	57.6	22.5	21.6	75.6	148.4	208.3	313.2	257.2	197	2.1	0	0	1303.5
2021	0.01	16.52	3.03	100.71	191.1	151.92	430.7	354.3	251.9	32.9	0	38.5	1571.59
2022	6.41	44.9	14.8	37.2	267.8	400.3	287.1	229.3	174.9	94	0	0	1556.71
Grand Total	**141.62**	**364.12**	**318.93**	**876.61**	**1667.2**	**2326.12**	**4593.5**	**4227.3**	**2392.9**	**544.3**	**36.1**	**75.4**	**17564.1**

Average	10.89384615	28.0092	24.533	67.432	128.25	178.932	353.35	325.18	184.0692	41.869	2.776923	5.8	1351.0846

Sum of Dhulikhel(Sum)	Column Labels												
Row Labels	January	February	March	April	May	June	July	August	September	October	November	December	Grand Total
2010	0	21.5	15	71	52	80	120	332	174.2	37.2	0	0	902.9
2011	3.5	47.3	16.3	64.2	207.9	267.4	287.3	276.2	257.4	4	26.5	0	1458
2012	9.9	27.2	1.2	98	36.1	110.9	423.2	0	210.1	0	0	0	916.6
2013	6.3	34.2	22.6	53.4	93.4	149.2	293.8	154.7	79.7	122.4	0	0	1009.7
2014	3	12.5	38.3	12.2	136.3	135.5	332	288.3	213.6	73.2	0	19.4	1264.3
2015	1.3	25.6	73	65.9	18.2	111.2	368.5	426.7	99.7	29.2	0	0	1219.3
2016	1.2	10.4	1.3	4.3	138.3	178.7	362.6	132	337.8	91.7	0	0	1258.3
2017	0	0	17.8	126.2	123.2	212.2	299.6	301.7	151.1	14.1	0	0	1245.9
2018	2.8	3.5	61.6	101.4	166.3	174.2	360.9	400.8	71.9	71.9	0	0	1415.3
2019	17.2	73.7	13.3	87.6	77.6	115.1	554.4	472.4	274.3	39.7	0	20.5	1745.8
2020	54.55	21.71	30.1	98	139.1	165.11	339.83	260.3	289.51	6	0	0	1404.21
2021	0.01	3.24	6.52	42.11	173.42	171.54	496.41	320	135.72	77	0	54.52	1480.49
2022	0.04	43.02	9.21	83.44	193.8	265.8	293.8	286.1	259.2	138.5	0	0	1572.91
			306.2	**907.7**	**1555.6**	**2136.8**	**4532.3**	**3651.**					
Grand Total		**99.8**	**323.87**	**3**	**5**	**2**	**5**	**4**	**2**	**2554.23**	**704.9**	**26.5**	**94.42**	**16893.71**
Avg	7.676923077	24.9131	23.556	69.827	119.663	164.373	348.642	280.86	196.4792	54.223	2.038462	7.263077	1299.5162

Sum of KhopASI	Column Labels												
Row Labels	January	February	March	April	May	June	July	August	September	October	November	December	Grand Total
2010	0	22	17	64	54	84	125.6	332.4	167.4	55.4	0	0	921.8
2011	0	47.8	9.4	69.6	188.2	293	225	245.4	257.2	35.4	22.8	0	1393.8
2012	8.2	31.8	1.4	81.6	37.4	43.6	283.6	175	51.4	8.6	0	0	722.6
2013	9.4	34.4	8.2	63.2	109.6	180	263.2	202.2	112	142.4	0	0	1124.6
2014	1.4	17	26	15.6	124.8	98.6	211.4	261.1	205.2	93.4	0	18.4	1072.9
2015	3.6	26.4	87.4	65	46.2	28.4	349.4	283.5	324.3	37.2	16	0	1267.4
2016	2.2	4.2	9.2	4.2	136.2	238	278.6	115.8	199.2	45	0	0	1032.6
2017	36.8	0	43.8	78.8	93.2	95.7	229	209.8	123.2	41.2	0	0	951.5
2018	1.8	2.6	41.6	81.8	145.8	257.8	303.4	405.2	22.8	10.2	0	0	1273
2019	19.2	67.4	32.6	57.6	55.4	124	418.4	162	254	51	0.5	23.1	1265.2
2020	80.2	23.2	24.6	106.6	178.3	209.2	247.6	206.8	48.6	0	4.81	3.22	1133.13
2021	56.5	223.93	168.92	424.33	267.63	100.72	56.92	0	54.2	1.8	47.61	2.01	1404.57
2022	34.7	119.82	201.32	220.61	255.53	186.22	110.11	0	0	14450.41	0	0	15578.72

Grand Total	**254**	**620.55**	**671.44**	**1332.94**	**1692.26**	**1939.24**	**3102.23**	**2599.2**	**1819.5**	**14972.01**	**91.72**	**46.73**	**29141.82**
Avg	19.53846154	47.7346	51.649	102.534	130.174	149.172	238.633	199.94	139.9615	1151.693	7.055385	3.594615	2241.6785

Data of Makwanpur in respect to each months

2010	3.5	0	0	67	165.5	39.5	96.9	317.3	374.2	149.5	7	1
2011	2.5	18.6	4	9.6	79.1	220.9	580.7	463.4	406.5	0	0	0
2012	19.5	42.4	0	40.2	72.8	0	744.2	409	349.4	11	2.5	0
2013	10.5	41.9	52.6	141.6	226.8	331.5	338.8	378.6	210.6	46.1	0	0
2014	12.9	16.5	1.4	4.5	109.6	85	311.3	487.9	214.1	177	1	6.9
2015	4.6	10.5	60.4	212.9	56	245.4	429.2	460.1	308.1	41.5	0	0
2016	17.8	9.5	0	27.5	259.6	289.5	608.4	413.7	245.2	163.1	0	0
2017	0	10.5	146.2	34	59.5	205.3	601.3	883.5	308.4	139.3	0	0
2018	5.5	0	0	31.5	123	439.7	250.6	282.8	212.4	14.5	0	0
2019	10.5	85.4	29.5	104.5	51	125.4	1371.1	459.4	755.6	40.3	0	23.2
2020	84.6	61.7	0	177.4	210.2	400.3	955.8	613.4	584	16	0	0
2021	0	0	4	8.5	442.7	413.7	934.91	705.3	367.1	309.1	11	12.5
2022	9.5	47.6	27.3	78.1	316.4	623.6	552.7	896.5	526	91.1	0	0

Data of Hariharpurgadhi in respect to each months

2010	0	5.5	28.2	39.1	406.3	281.3	521.8	715.9	427.2	157.7	0	0
2011	0	34.2	18.7	124.1	191.7	522.1	673	368	553.8	9	19.6	0
2012	16.7	11	2.1	98.5	100	426.7	614.9	568.9	363.9	19.1	0	0
2013	3.1	36.5	5.5	131.2	307.6	519.3	587.9	287	351.6	106.5	0	0
2014	4.3	10.2	0	8.9	215.1	438.9	617.9	734	376	64	0	6.7
2015	6.6	10.3	52.5	61.4	123.7	438.7	595.4	687	249.5	16.5	0	0
2016	28	4.3	36.7	0	204.3	383	601.3	346.2	306.1	123.6	0	0
2017	5	0	59.9	64.7	210.5	331.8	424.7	776.3	445.6	276.6	0	0
2018	0	1.1	2.5	102.5	167.8	434.4	623.4	773.5	391.3	20.5	0	0
2019	4	64.3	7.7	127.7	80.1	230.4	1180.9	265.7	471.5	68.6	0	26.2

2020	50.2	17.2	75.2	130.4	195.9	375.2	1033.4	314	484.1	34.1	0	0
2021	0	0.02	1.7	38.13	333.63	271.93	758.15	640.7	382.76	215.61	0	27.31
2022	2.13	38.02	5.32	60.63	301.64	864.95	314.75	368.9	348.71	128	0	0

Annexes-3

Photographs

Figure: Landslide observed in kholsi

Figure Crack observed

Figure: Fold observed